# Demonstration of an Efficient Ambient Radio-frequency and Microwave Energy Harvesting System with High Sensitivity and DC Output

A Thesis

Presented to

the faculty of the School of Engineering and Applied Science

University of Virginia

in partial fulfillment
of the requirements for the degree

Master of Science

by

Siyi Shen

December 2017

# APPROVAL SHEET

This Thesis
is submitted in partial fulfillment of the requirements
for the degree of
Master of Science

Author Signature: ______________________

This Thesis has been read and approved by the examining committee:

Advisor: N. Scott Barker

Committee Member: Steven M. Bowers

Committee Member: Robert M. Weikle

Committee Member: ______________________

Committee Member: ______________________

Committee Member: ______________________

Accepted for the School of Engineering and Applied Science:

Craig H. Benson, School of Engineering and Applied Science

December 2017

# Abstract

## Demonstration of an Efficient Ambient Radio-frequency and Microwave Energy Harvesting System with High Sensitivity and DC Output

Directed by: Professor N. Scott Barker

The great potential to harvest and utilize ambient Radio-frequency and microwave power has led to much research as the occurrence of a worldwide coverage of radio waves during the past decade. However, RF harvesting circuits have already been proved for more than a half century, only a small number of them have been able to be activated freely without dedicated sources and harvest available ambient RF energy that typically has a power density ranging from 0.001 to 0.1 μW/cm$^2$.

This thesis presents a detail description of each element of an RF energy harvesting system operating at 2.45 GHz, including an antenna, an RF-to-DC conversion rectifier and an integrated module of DC-DC up-conversion and power management. This thesis does not focus on the design of the antenna and the integrated module, both of which are products designed by Texas Instruments.

The key section of this thesis is concerned about the RF-to-DC rectifier, which is the core part that converts collected RF power to applicable DC power. In this section, the reasons that only a small number of rectifiers can work efficiently with ambient RF power levels are presented based on nonlinear model analyses of a diode, the dominant rectifying device in RF and microwave power harvesters. And the mechanism of overall power conversion efficiency (PCE) of the rectifier is explained in this analysis. Besides, a prototype of a modified rectifier is designed, fabricated and measured to demonstrate the potential ability to work in ambient power regions.

The entire RF energy harvesting system is tested with an RF signal generator at the end of this thesis. The overall efficiency of the harvester can reach 5.17% to deliver a DC output voltage of 1.8 V with an incident power of -10 dBm. And it can have an estimated efficiency of 13% to output a high DC voltage of 4.2V when charging a rechargeable battery MS920SE with the same power. At last, a comparison among power harvesters is given, showing a performance of high sensitivity and DC voltage output of this work in the mode of battery charging. Potential solutions to some unsolved issues in this thesis have been discussed and can be further studied in future works.

# Contents

# Chapter 1. Introduction

## 1.1 Background of Wireless Power Transmission and RF energy harvesting

Radio Frequency/Microwave energy is currently available all around the world, transmitted from ubiquitous energy sources, including mobile phones, cellular base stations, radio/television broadcast stations and Wi-Fi routers [1]. In the process of wireless power transmission (WPT), energy sources transmit excess energy that is not utilized in communications.

The potential to harvest and utilize RF energy for emerging low power applications, from the excess energy in the surroundings, has been supposed to have a promising prospect and inspired research interests exponentially.

Essentially, WPT can be divided into three types [2]: (a) inductive, capacitive or resonant reactive near-field coupling; (b) far-field directive power beaming; and (c) far-field nondirective power transfer.

In the first type, the near-field coupling is typically accomplished through magnetic fields with a transformer. Power is transferred between two coils that resonate at the same frequency. The power conversion efficiency of this method depends critically on the coupling between the coils, and therefore their position, with expected high efficiency for high-Q resonant transformers [2]. The main practical reason for this type of power transfer is to eliminate the inconvenience of contact. And a number of commercial products have been available over the past decades.

The second type of WPT is to transfer power by propagating radio waves, radiated and received through antennas in a well-defined direction [3], [4]. The directive wireless powering has already been a topic of research for decades. W.C. Brown is a pioneer in this field who made important contributions to this emerging technology. He demonstrated a helicopter that received all the power needed for flight from a microwave beam for up to 10 h [4]. The efficiency of this wireless powering is lower and does not necessarily depend critically on placement of antennas. The high efficiency comes from the specific design of antenna arrays for different applications [3], [4].

At last, the third type of WPT is the nondirective power transfer. Typically, this type has three key features [2]: 1) the available incident power densities are low; 2) the frequency range of power sources harvested can vary from narrowband to broadband 3) The position of the transmitters and receiving devices may vary and is not particularly designated.

This thesis focuses on the last type of WPT. RF energy harvesting circuits have been demonstrated for more than 50 years, but only a few have been able to harvest energy from freely available ambient RF sources [5]. This thesis will first analyze and clarify the reason for that limitation and then verify the ideas that improve the performance of RF harvesting circuits.

### 1.2 A Brief History and literature review

Essentially, the research topic of ambient RF and microwave power harvesting is a branch of wireless power transmission that is first experimentally demonstrated by Nikola Tesla in 1899 [6]. He actually built a gigantic coil that was connected to a 200 ft high mast with a 3 ft diameter ball at its top, which was called the “Tesla Tower”. Unfortunately, the experiment failed because the transmitted power was diffused in all directions using 150 kHz signal, whose wavelength was around 2 km.

After that, especially in the 1960s, W.C. Brown introduced the first research and development on Microwave Power Transfer (MPT) that is WPT using microwaves [3]. As is mentioned above, during this period, applications have been developed considering high power transmission, including solar-charged satellite-to-ground communication systems and helicopters powered by microwave beams. First in 1963, Brown developed the first rectifying antenna for helicopters, whose efficiency was 50% at a DC output of 4W and 40% at a DC output of 7W [6]. Then in the 1970s, Brown attempted to increase the total RF–DC efficiency using 2.45 GHz microwaves. But the overall efficiency decreased a lot at 2.45 GHz, where the overall RF–DC efficiency was only 26.5% at a DC output of 39 W in the Marshall Space Flight Center tests of 1970 [6].

Then after the mid-1980’s, the idea of RF energy harvesting is implemented significantly in radio-frequency identification (RFID) [7]. The first developed tags were passive and Read-only (R/O). They were battery free, powered by the signal from the reading device. Tags are permanently uniquely coded during manufacture with a 64-bit binary number. For example, the work shown in [42] presents a new passive UHF RFID Transponder IC with a sensitivity of 16.7 µW. This transponder has a reading distance of 4.5 m at 500-mW ERP or 9.25m at 4W EIRP base-station transmit power. The overall efficiency is around 5% at an incident power of -13.5 dBm. Other demands from industrial and biomedical fields, to monitor physical or environmental conditions, such as temperature, sound, pressure, etc. and to collect, share and analyze their data through a network, have also inspired the interests on low power harvesting for wireless sensor network (WSN) [8]. The work [18] has focused on a variety of issues related to energy harvesting techniques and proposed the study and design of rectifier and DC/DC converter topologies for energy collection and DC voltage boosting in self-powered WSN application.

Recently, numbers of works that were carried out in the past decade have introduced and developed the performance of total RF power harvesting systems or certain parts in those systems. For example, K. Gudan and his group proposed two RF energy harvesting and storage systems. The former system flows 5.8 micro-joules into a rechargeable NiMH battery after 1 hour at -20dBm RF input power at 2.45 GHz, as shown in Figure 1(a) [9]. The latter one was improved that enables battery charging from incident power levels as low as -25 dBm operating at 2.4 GHz, accumulating 2 micro-joules in the same battery in one minute when -25 dBm power is incident, as shown in Figure 1(b) [10]. And later they modified the whole system adding an auxiliary control system, as shown in Figure 1(c) [11]. Experimental results revealed that the system stores 241µJ into a NiMH battery after 30 minutes with an incident power of -21 dBm.

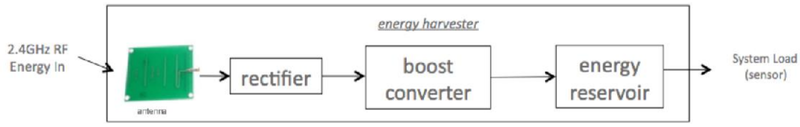


(a) Work [9]

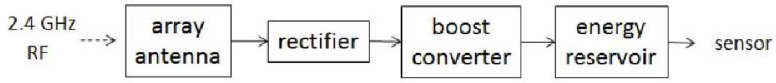


(b) Work [10]

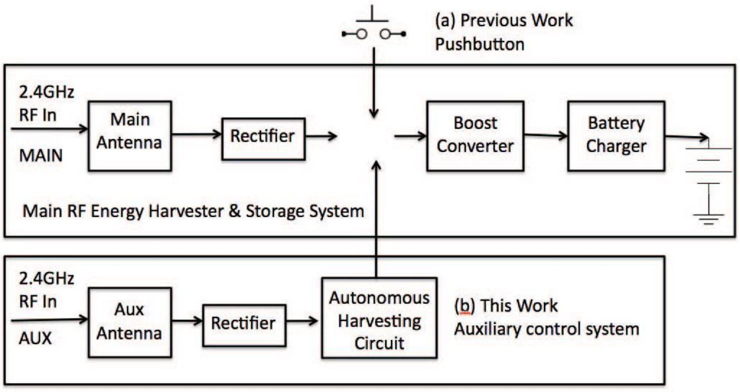


(c) Work [11]

Figure 1. The structure of RF harvesting System reproduced from [9], [10], [11]

On the other hand, most of groups concentrate on RF-to-DC rectifier, a critical part of an RF energy harvester. The most essential parameter to evaluate the performance of a rectifier is power conversion efficiency PCE. Especially, Simon Hemour, Carlos Henrique Petzl Lorenz and their team have outstanding works on theoretical analysis of power conversion efficiency based on the square-law rectification model [12]. Meanwhile, they made a list summarizing PCE, operating frequency and rectifying devices of all the works related to RF rectifiers recently and a graph showing all these curves of rectifiers' PCE versus input power. Besides, they predicted better performance of rectifiers using different tunneling diodes [13] and built a rectifier with heterojunction backward tunnel diodes that indicated relatively high PCE at ultra-low incident power, with a total power conversion efficiency of 3.8% for -40 dBm input power and 18.2% for -30 dBm input power at 2.35 GHz [14].

Moreover, some other groups [15] focused on the low power DC-DC converter based on previous designs for other types of sources such as thermoelectric, microbial electric generators and so forth [16], [17]. Experimental results illustrated that converter efficiency reaches a maximum of 25% for input power levels between

60μW and 200μW. For power levels from 5μW to 1mW, efficiency is between 10% and 25%. However, there are hardly high-sensitivity DC-DC boost converters working efficiently with input power levels below 1 μW. So the DC-DC boost converter can be a promising topic in the future.

### 1.3 Outline of thesis

In this thesis, studies were conducted to realize and evaluate an RF harvesting system that is potentially possible to collect ambient RF energy.

Chapter 2 provides an overview of components of a general RF energy harvesting network, including an antenna, a RF-to-DC rectifier, a power management module and a storage device. And two critical issues in the design for ambient RF power levels are discussed.

Chapter 3 provides the topology of a commercially available inverted F antenna, from which the fabricated antenna in this thesis is modified. The results of simulated port parameters, radiation patterns of field strength and polarization directivity using HFSS are illustrated, while only the results of measured port parameters are given due to the limitation of conditions.

Chapter 4, the core in the thesis, theoretically discusses the RF-to-DC power conversion efficiency with a square-law rectification model and presents the comparison of simulations and measurements of designed RF rectifier. Simulations are conducted using Microwave office and data processing using Matlab.

Chapter 5 describes a commercial product of a boost converter and power management module. The DC-DC conversion efficiency are measured with two source-meters.

The last chapter shows the working performance of the entire RF harvesting networks and conclusions as well as the discussion of future works. Summarized statements are given at the end.

# Chapter 2. Overview of RF energy harvesting systems

## 2.1 Architecture of RF Energy Harvesting Systems

Figure 2 shows the block diagram of the RF energy harvesting system in this thesis. The RF energy harvesting network consists of the following major components:

1) A receiving antenna. The antenna can be designed to work on either single frequency or multiple frequency points, either narrow or broad frequency bandwidth. Thus the network can harvest from a single or multiple sources simultaneously. As a matter of fact, the RF energy harvester typically operates over ranges of frequencies since energy density and sources of ambient or dedicated RF signals are diverse in frequency. Besides, especially for the purpose of ambient power harvesting, an omnidirectional antenna or antenna array with high performance is desired to gather as much power as possible.

2) An RF energy harvester / converter, composed of an RF antenna, an impedance matching, an RF-to-DC rectifier and a load capacitor, to collect excess RF signals and convert them into DC energy.

3) A power management module that decides whether to either store the electricity obtained from the RF energy harvester to a rechargeable battery or a supercapacitor, or to utilize it for low-power or battery-free applications such as wireless sensor networks [8], [18], wearable radio platforms [19]. Generally, a DC-DC converter that transfers the energy from a harvester to usable energy for various applications is integrated in this power management module.

4) A low-power microcontroller that is attached to tune upper and lower threshold voltage ranges for protection of storage devices or loads of applications.

5) A cold start-up circuit that is used to activate the microcontroller, keeping the current flows stable out of the power management module. The start-up circuit usually receives energy from a RF-to-DC rectifier or an antenna [11], [20].

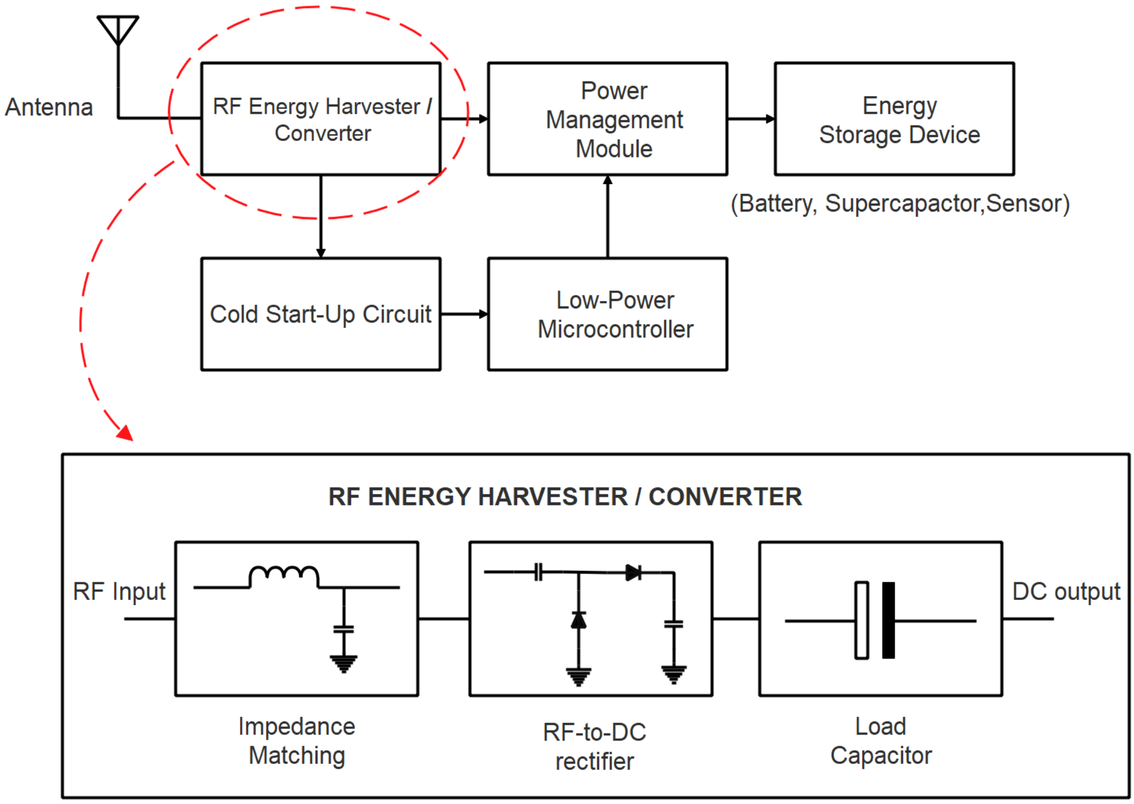


Figure 2. The block diagram of a general architecture of an RF energy harvesting network.

Figure 2 also in detail illustrates the block diagram of the typical RF energy harvester, which consists of an impedance matching network, an RF-to-dc rectifier, a load capacitor.

a) The impedance matching is a resonator circuit operating at the designed frequency to maximize the power transfer between the antenna and the RF-to-DC rectifier. The efficiency of the impedance matching is not high at the designed frequency because of the decreasing quality factors of LC components. And it depends significantly on the matching topology.

b) The main component of the RF-to-dc rectifier is diodes which convert ambient or dedicated RF signals into DC voltage. Generally, higher power conversion efficiency can be achieved by special diodes with lower built-in voltage and parasitic resistance [12], [13], [14]. The load capacitor ensures to deliver power smoothly to the system load. Additionally, when RF energy is unavailable, the capacitor can also serve as a reserve for a short duration.

## 2.2 Design issues in an RF energy harvesting system

### 2.2.1 Consideration of ambient RF power density

First of all, the essential problem in energy scavenging applications is the energy that can be extracted and collected for power conversion in an energy harvesting system. In recent decades, technologies such as wind turbines, hydro-electric generators and solar panels have been developed and turned harvesting into a small but growing contributor to the world's energy requirements. Scavenging energy from RF emissions is interesting, but the energy availability might be less than one hundredth of the magnitude of the former three forms of energy [21].

Table 1 shows the estimated harvested power for different kinds of energy sources from previous studies and measurements. The referred power density from RF/EM harvesting in the table is the average power that can be collected from public services except for the dedicated energy sources.

Table 1. Estimated Power density of energy harvesting [21], [22]

| **Energy Source Harvested Power** | | **Harvested Power** |
|---|---|---|
| **Vibration/Motion** | Human | $4\ \mu W/cm^2$ |
| | Industry | $100\ \mu W/m^2$ |
| **Temperature Difference** | Industry | $1 - 10\ mW/cm^2$ |
| **Light** | Indoor | $10\ \mu W/cm^2$ |
| | Outdoor | $10 mW/cm^2$ |
| **RF/EM** | GSM | $0.1\ \mu W/cm^2$ |
| | Wi-Fi | $0.01\ \mu W/cm^2$ |
| **Solar** | Outdoor | $10\ mW/cm^2$ |
| | Indoor | $<\ 0.1\ mW/cm^2$ |
| **Acoustic** | 75 – 10 dB of noise | $0.003 - 0.96\ \mu W/cm^2$ |
| **Human Body Sources** | Body heat | $0.2 - 0.32$ W (neck) |
| | Walking | $5 - 8.3$ W |

Additionally, some papers have been published concerning the measurements of RF power levels at certain locations [5], [23].

In [5], electric field strength was measured between 0.3-2.5 GHz using an Agilent N9912A FieldFox RF analyzer with a calibrated Aaronia BicoLOG 20300 omnidirectional antenna. The input RF power density is then calculated from the electric field strength measurement. Figure 3 shows the input RF power density measured outside the Northfields London Underground station. From the spectrum of power density, bands of DTV, GSM900, GSM1800, 3G, and Wi-Fi can been clearly identified. The average power density of GSM900 and Wi-Fi is $36\ \mathrm{nW/cm^2}$ and $0.18\ \mathrm{nW/cm^2}$, respectively.

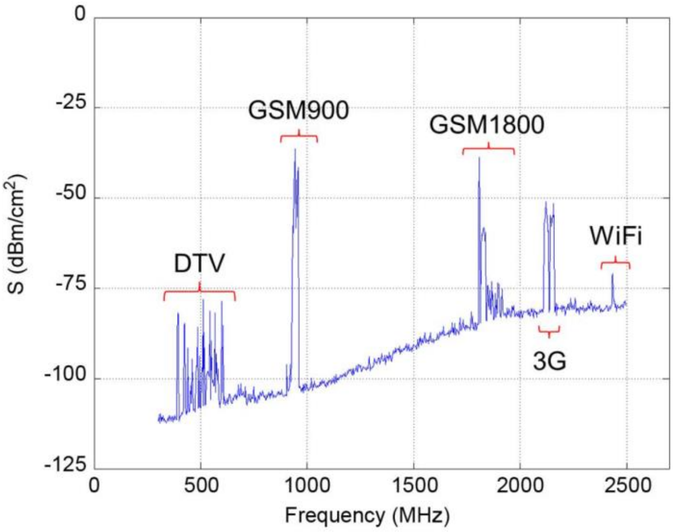


Figure 3. Input RF power density measurements outside the Northfields London Underground station. Image reproduced from [5].

On the other hand, Figure 4 shows the measurements of peak power density in GSM-900 and Wi-Fi band [23]. In GSM-900, for distances ranging from 25m to 100m from a GSM base station, power density levels ranging from $0.01\mathrm{mW/m^2}$ to $1\mathrm{mW/m^2}$ may be expected for single frequencies.

And the measurements of Wi-Fi power density is carried out in the building of Electrical Engineering in Eindhoven University of Technology. The measured power density within a distance of 10 meter is very close to the estimated value in Table 1, as shown in Figure 5.

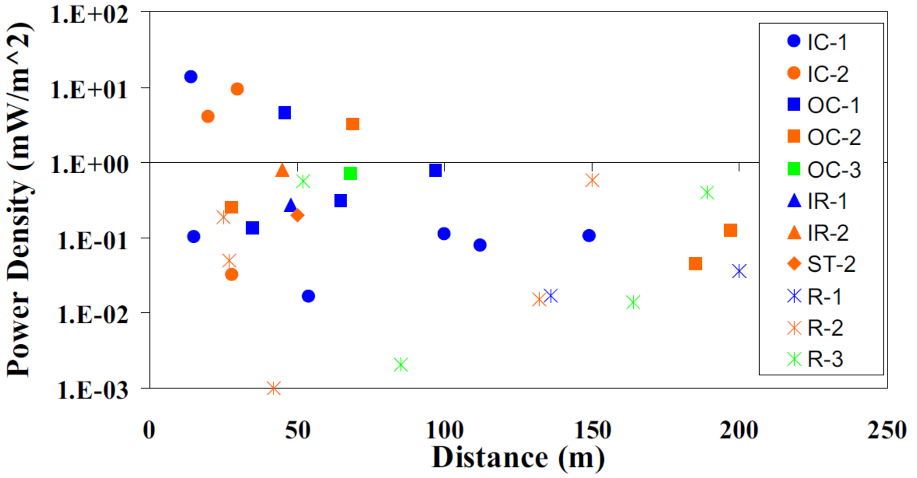


Figure 4. Measured GSM-900 peak power density levels as a function of distance to the nearest base station. Data from ground level measurements is removed. Code 'XY-a' indicates area and measurement site characteristics. XY: IC=Inner City, OC=Outer Country, IR=I Industrial area, ST=Small Town, R=Rural or country-side; a: 1=outdoors on roof, terrace or balcony, 2=indoors, close to windows, 1.5m or less, 3=indoors, not close to windows. Image reproduced from [23].

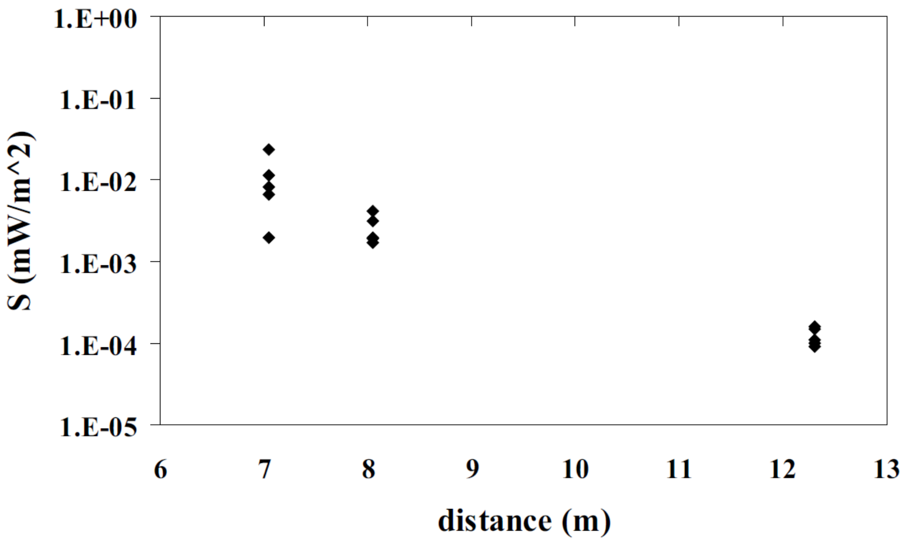


Figure 5. Measured WLAN peak power density levels as a function of distance to the nearest WLAN router. Image reproduced from [23]

Besides, the collected power from Wi-Fi routers is generally not steady. The emitted waveform from a Wi-Fi router is discrete and shows burst peaks in a short duration. As a result, the low power microcontroller cannot work in a steady state to drive the power management module.

### 2.2.2 RF-to-DC power conversion efficiency

Recently, most RF harvesters presented in the papers have been evaluated using dedicated sources rather than harvesting from ambient RF energy [5]. Only few of them could work well without dedicated signals as a whole system. However, the power sensitivity of those systems, that the minimum power level to activate and enable harvesting, is ranging from -25 to -12 dBm [10], [24], [25], [26], which is still much higher than a general value of ambient power density.

In recent years, high efficiency RF harvesters have been demonstrated with relatively high input RF power levels (typically larger than 0 dBm) such as 78% [27] and 90% [28]. Nevertheless, few of scholars have studied and fabricated RF harvesters with convincing values of efficiency given ultra-low power levels that can be collected without dedicated sources (typically lower than -30 dBm). The reasons can be foreseen with a series of mathematical analyses and are presented in the Chapter 4 of this thesis.

# Chapter 3. Antenna design for energy harvesting

In this chapter is described the design topology, simulations and fabrication of a printed inverted-F antenna centered at 2.4 GHz. This antenna is compact, low cost, and high performance, whose dimensions are exactly duplicated according to the application report *SWRU120C* of Texas Instruments [29]. But the feed point is modified for the convenience of test. First we start with a brief explanation of the parameters of an antenna then we briefly explain the advantages of using this type of antenna. Also a brief introduction of the design and simulations. Measurements are given but radiation patterns are not available without an anechoic chamber.

## 3.1 Topology of Antenna

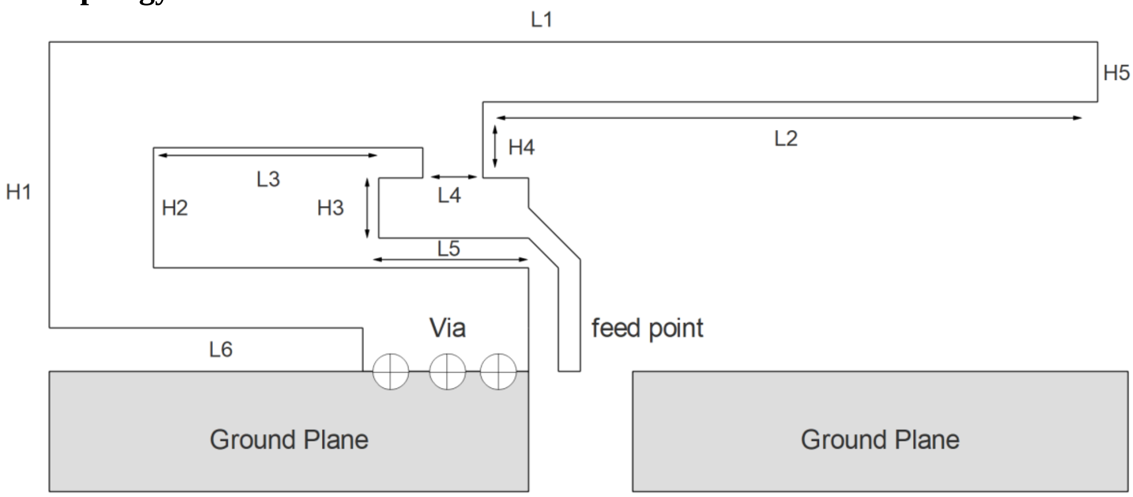


Figure 6. Layout pattern of the Inverted-F antenna

The layout pattern of the selected Inverted-F antenna is illustrated in Figure 6, where all dimensions are listed in Table 2. There is no ground plane beneath the antenna pattern, so the PCB substrate thickness will have little effect on the performance [29]. The ground plane is set to be as wide as the length of the antenna, and the height of ground plane is larger than a quarter wavelength otherwise the bandwidth will decrease. The results presented in this chapter are based on an antenna implemented on a FR-4 ($\varepsilon_r \cong 4.4$, $tan\delta \cong 0.02$) PCB with a thickness of 62 mil.

Table 2. Dimensions of the Inverted-F antenna

| | | | |
|---|---|---|---|
| L1 | 25.58 mm | H1 | 6.17 mm |
| L2 | 16.40 mm | H2 | 2.67 mm |
| L3 | 4.80 mm | H3 | 1.21 mm |

| | | | |
|---|---|---|---|
| L4 | 1.20 mm | H4 | 1.80 mm |
| L5 | 3.20 mm | H5 | 1.21 mm |
| L6 | 6.98 mm | | |

### 3.2 Advantages and disadvantages

An antenna for an RF energy harvesting system is often connected directly to the input port of an RF-to-DC rectifier, which is referred as a “rectenna” in an RF power harvester. The inverted-F antenna is compact in size so that convenient to be integrated with a rectifier and possible to optimize the size as well as the performance of the overall RF harvesting circuit. This is an essential reason for choosing this type of antenna in this thesis. And according to the design and measurement in application report [29], the antenna has a good radiation pattern and the maximum gain is measured to be +3.3 dBi.

However, the inverted-F antenna is compact, which means that this antenna will be less efficient than some other types of antenna. Meanwhile, the substrate used in this thesis is FR-4 that having a high loss tangent of 0.02. The total gain is decreased due to high loss in dielectric.


Figure 7. Fabricated antennas with modification on feed points

### 3.3 Results

Both Simulated and Measured return losses of antennas at 2.4 GHz are displayed in Figure 8. The bandwidth of both two fabricated antennas is decreased. The possible reasons are the mismatch caused by modification of feed points and a larger size of substrate used in prototype.

Figure 9 and Figure 10 are the three-dimension display of radiated E-fields and total gain in simulation, respectively, where the maximum gain is around +1.97 dBi.

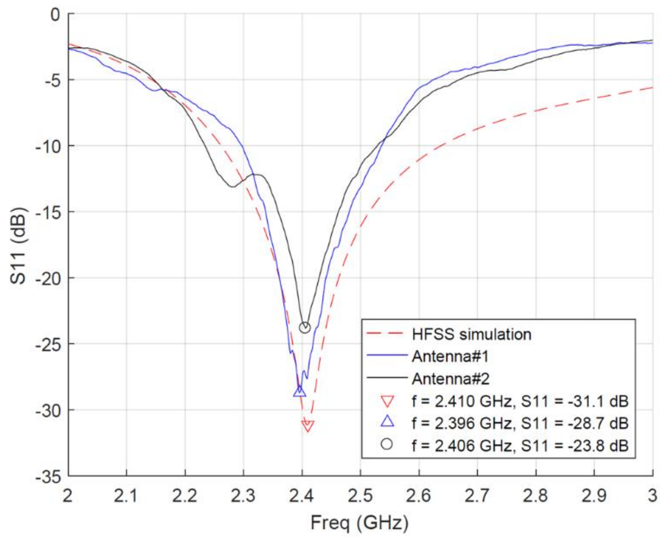


Figure 8. Simulated and Measured return losses of antennas at 2.4 GHz

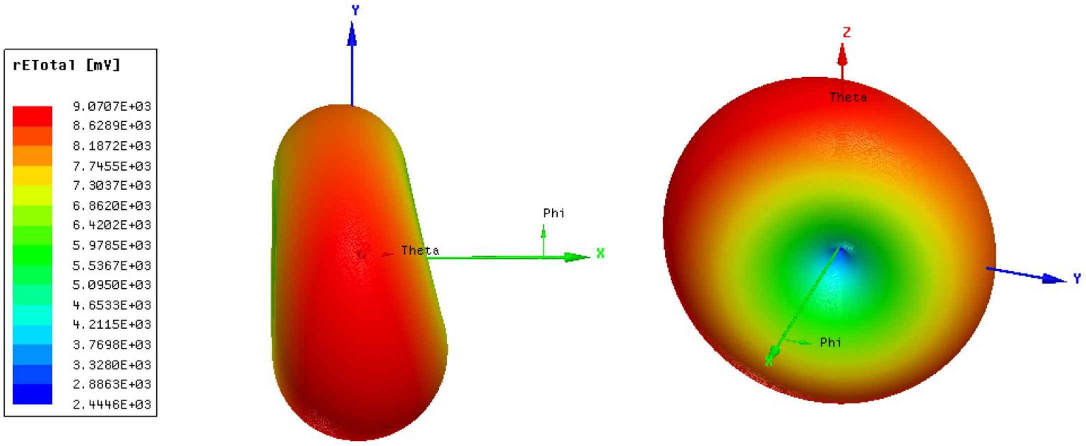


Figure 9. Radiated E-fields of the antenna at 2.4 GHz in simulation

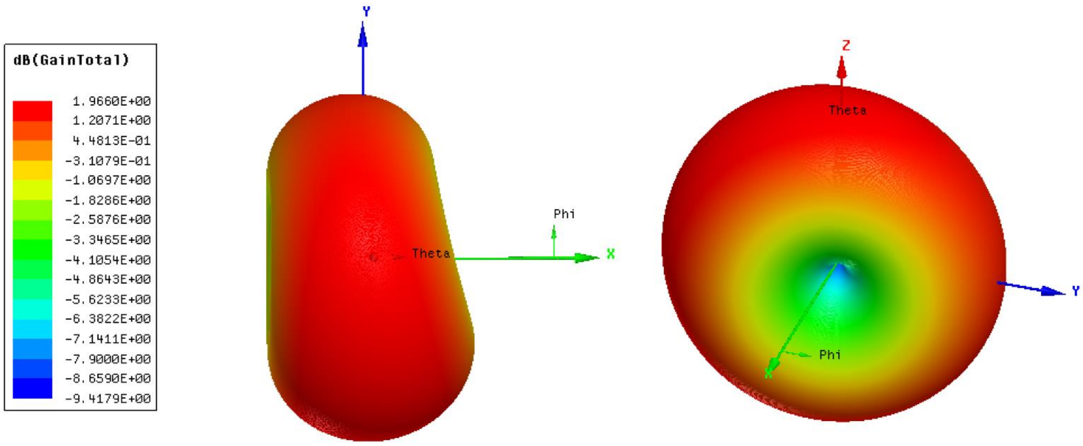


Figure 10. Simulated three-dimension total gain of the antenna at 2.4 GHz

And Figure 11 shows the simulated gain pattern of the antenna for both E-plane and H-plane at 2.4 GHz. The two curves with brighter colors represent the E-plane radiation pattern for $\varphi = 0$ or $90^{\circ}$ while the rest ones with darker colors represent the H-plane radiation pattern for $\varphi = 0$ or $90^{\circ}$. But it should be mentioned that the radiation patterns of E-plane and H-plane with the same value of φ are not very similar. The explanation is that the isolation of the antenna is reduced with the implementation of the type of printed antenna and the modification of antenna port.

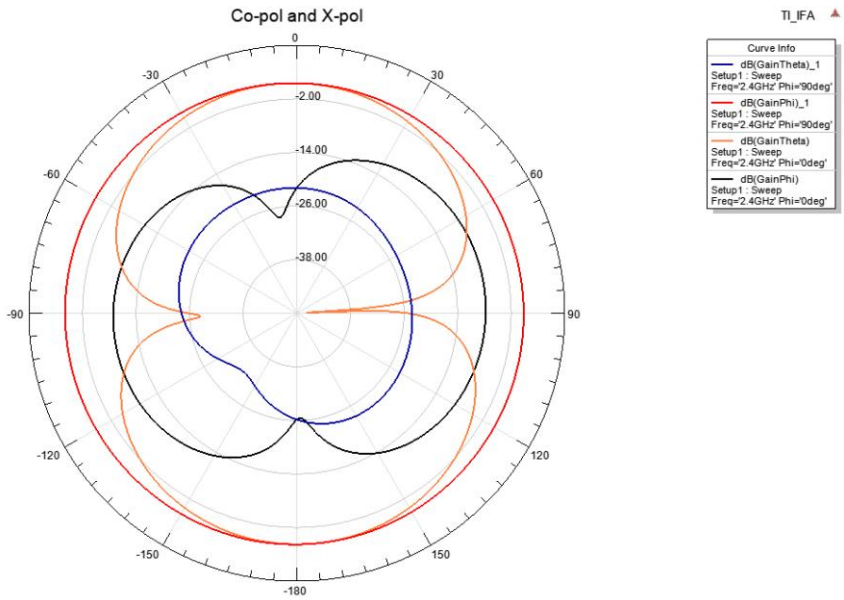


Figure 11. The simulated radiation pattern with co-polarization and cross-polarization at 2.4 GHz

# Chapter 4. RF to DC conversion

This chapter mainly focuses on the design of the RF-to-DC rectifier, where the chief issue is to acquire the RF-to-DC power conversion efficiency (PCE) as highly as possible. Firstly, in this chapter, mathematical analyses of the power conversion efficiency are presented to explain the reason why only a few RF energy harvesting circuits are able to harvest energy from freely available ambient RF sources after developments for decades of years.

Next, two types of rectifiers, the half-wave and full-wave rectifier, are mentioned and simulated in design. And a modified full-wave rectifier is fabricated and measured to verify the design. Analyses are also listed to explain the discrepancy between measurements and design simulations, which are probably challenges or motivations for potential topics and further research in future works.

## 4.1 Physical Limitations of RF Rectification

In RF energy harvesting applications, the expected operation power has a maximum level reaching -15 dBm in high power density regions, but a typical average power of only -30 dBm and below in most areas with low-density ambient power [5], [18], [30]. At these power levels, previous works have presented enough evidence that demonstrates deficient PCE of rectification at high frequency microwaves [20], [31], [32].

Therefore, the “low-power barrier” of PCE of a rectifier plays a negative role in the energy rectification process to utilize much more power. In order to get a PCE as high as possible with a limited manufacturing condition (that using substrate material FR-4 for the sake of saving budget), it is necessary to understand the low power level mechanism inside rectifiers, i.e., diodes used essentially.

Previous works [12], [14] have demonstrated a good approximation using the square-law power rectification model that neglecting higher order harmonics inside diodes. In this rectification model, the power conversion efficiency mechanism is divided into several steps, each one with an intrinsic efficiency. The total PCE can be calculated using the expression below (1) [12]

$$PCE = \frac{P_{DC}}{P_{RF}} = \eta_M \cdot \eta_p \cdot \eta_0 \cdot \eta_{DC-transfer} \tag{1}$$

where $P_{DC}$ is the dc power delivered to the load of the rectifier, $P_{RF}$ is the input power, $\eta_M$ is the matching network efficiency, $\eta_p$ is the parasitic efficiency, $\eta_0$ and $\eta_{DC-transfer}$ is the nonlinear junction RF-to-dc power conversion efficiency.

### 4.1.1 Matching Efficiency $\eta_M$

RF and microwave signal experiences reflection when it enters into a device with different impedance. The reflections can be well eliminated using a matching network at the expense of narrowing operating frequency bandwidth. The matching efficiency comes from the resulting insertion loss of the matching network. And this efficiency can vary depending significantly on the concrete matching topologies, required quality factor Q, etc.

For the case of a simple L-matching network, the insertion losses can be calculated using the required quality factor of matching circuit $Q_r$ and the obtained quality factor $Q_m$ [12], [14], [33], using the following equations:

$$\eta_M = \frac{1}{1 + \frac{Q_r}{Q_m}} \tag{2}$$

$$Q_r = \sqrt{\frac{R_{High}}{R_{Low}} - 1} \tag{3}$$

where $Q_r$ is the required quality factor, which depends on the mismatch between the highest impedance $R_{High}$ and lowest impedances $R_{Low}$ that are to be matched. In our case of rectifier matching, this is typically the port impedance 50 Ω and the diode's junction resistance.

Therefore, it is obvious to notice from equation (2), (3) that high zero-bias junction resistance diodes cannot be used because of large losses in the matching network, resulting from a larger mismatch between a lower source impedance and a larger junction impedance. For this reason, previous works of RF energy harvesting circuits usually involves diodes like Skyworks SMS7630 or Avago HSMS-2850, HSMS-2860 series [1], [9], which have relatively low zero-bias junction resistances, in the order of few kΩ.

### 4.1.2 Diode Parasitic Efficiency $\eta_p$

In the case of diodes, which are the subject of the study presented in this thesis, the equivalent diode circuit model with package parasitic components is used [4], as shown in Figure 12. In this figure, $R_j$ represents the diode's nonlinear junction resistance, $C_j$ the junction capacitance, $R_s$ the series resistance inside diode, $C_p$ the package parasitic capacitance and $L_p$ the parasitic inductance. The junction resistance $R_j$ is a function of the dc current flowing through the junction $I_{bias}$ that can be easily extracted from the measurement of I-V characteristics.

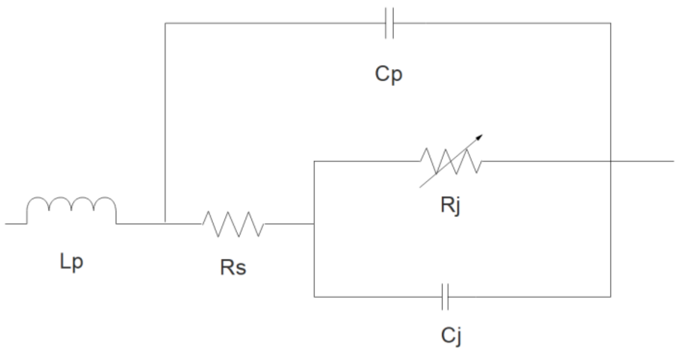


Figure 12. Equivalent circuit model of a diode

Apparently, a portion of the incident energy is dissipated in the parasitic resistance $R_s$ that comes from manufacturing process and package of the device. And another part of energy passes through the nonlinear junction of the diode, which means that the part of energy cannot be converted.

Using the model shown in Figure 12 above, the parasitic efficiency can be calculated. First, the current that flows through this nonlinear junction is expressed, where $V_b$ represents the voltage across the junction:

$$I_{tot} = \frac{V_b}{Z_j} = \frac{V_b}{R_s + \frac{1}{1/R_j + j\omega C_j}} \tag{4}$$

Thus, the total power that gets into the diode is obtained:

$$P_{tot} = Re\left(\frac{{V_b}^2}{Z^*}\right) = {V_b}^2 \frac{R_s + R_j + R_s \cdot (\omega C_j R_j)^2}{(R_s + R_j)^2 + (\omega C_j R_j R_s)^2} \tag{5}$$

On the other hand, the current that flows into the junction resistance $R_j$, is divided by a voltage divider comprised of $R_j$ and $C_j$:

$$I_j = I_{tot} \cdot \frac{1/j\omega C_j}{R_j + 1/j\omega C_j} = \frac{V_b}{R_s + R_j + j\omega C_j R_j R_s} \tag{6}$$

The power absorbed by the junction resistance $R_j$ is then calculated below:

$$P_j = |I_j|^2 R_j = {V_b}^2 \cdot \frac{R_j}{(R_s + R_j)^2 + (\omega C_j R_j R_s)^2} \tag{7}$$

Above all, with the assumption that the condition of $R_j \gg R_s$ exists at zero-bias, the parasitic efficiency of rectifying diode is

$$\eta_p = \frac{P_j}{P_{tot}} = \frac{1}{(1 + (\omega \cdot C_j)^2 \cdot R_j \cdot R_s)^2} \tag{8}$$

### 4.1.3 RF-to-DC conversion efficiency $\boldsymbol{\eta_0 \cdot \eta_{DC-transfer}}$

The nonlinearity of a rectifying diode can be described by dc the voltage – current equation. The voltage can be expanded in Taylor series about $I_{bias}$

$$v(i) = v(I_b) + v'(I_b) \cdot (i - I_b) + \frac{v''(I_b)}{2} \cdot (i - I_b)^2 + \cdots \tag{9}$$

If an RF current of magnitude *M* and frequency *ω*

$$i_\omega(t) = M \cdot \cos(\omega t) \tag{10}$$

Flows through a perfectly matched junction, the resulting voltage of the junction can be calculated by replacing *i by* $i_\omega(t)$ in equation (9) above.

$$v(i) = v(I_{bias}) + v'(I_{bias}) \cdot (i - I_{bias}) + \frac{v''(I_{bias})}{2} \cdot (i - I_{bias})^2 + \cdots$$

$$= v(I_{bias}) + v'(I_{bias}) \cdot [M \cdot \cos(\omega t) - I_{bias}] + \frac{v''(I_{bias})}{2} \cdot [M \cdot \cos(\omega t) - I_{bias}]^2 + \cdots$$

$$\begin{aligned} &= \left[ v(I_{bias}) - v'(I_{bias}) \cdot I_{bias} + \frac{v''(I_b)}{2} \cdot {I_{bias}}^2 + \frac{v''(I_{bias})}{4} \cdot M^2 \right] \\ &+ [v'(I_{bias}) - v''(I_{bias}) \cdot I_{bias}] \cdot M \cdot \cos(\omega t) + \frac{v''(I_{bias})}{4} \cdot M^2 \cdot \cos(2\omega t) \end{aligned} \tag{11}$$

Keeping the only term for which $\omega = 0$, the rectified voltage is

$$v_{rect} = \frac{1}{4} \cdot M^2 \cdot \frac{d^2 v(I_{bias})}{di^2} \tag{12}$$

In the equation (12) above, it is assumed that no power goes into the higher order harmonics, i.e. neglecting higher order terms in the Taylor series (9).

On the other hand, keeping the term relating to $\omega$ will give the RF voltage across the junction

$$v_\omega(t) = M \cdot \cos(\omega t) \cdot \frac{dv(I_{bias})}{di} \tag{13}$$

that leads to the RF power absorbed by the rectifying diode. Briefly, RF power is an integration of the product of the RF current and voltage over a period T

$$P_\omega = \frac{1}{T} \int_0^T v_\omega(t) \cdot i_\omega(t) \cdot dt$$

$$= \frac{1}{T} \int_0^T M^2 \cdot \cos^2(\omega t) \cdot \frac{dv(I_{bias})}{di} \cdot dt$$

$$= \frac{1}{T} \cdot M^2 \cdot \frac{dv(I_{bias})}{di} \int_0^T \frac{1 + \cos(2\omega t)}{2} \cdot dt$$

$$= \frac{M^2}{2} \cdot \frac{dv(I_{bias})}{di} \tag{14}$$

The ratio of the output dc voltage by the absorbed RF power is defined as voltage responsivity. The responsivity of a diode is usually expressed in units of either amperes or volts per watt of incident radiant power [12].

$$\Re_v = \frac{v_{rect}}{P_\omega} \tag{15}$$

The open circuit voltage responsivity $\Re_v$ can be linked to the short-circuit current responsivity $\Re_i$ by the differential junction resistance $R_j = dv(I_{bias})/di$

$$\Re_v = \Re_i \cdot R_j \tag{16}$$

With equation (12) (14) (15),

$$\Re_v = \frac{1}{2} \cdot \frac{v''}{v'} = \frac{1}{2} \cdot \frac{dR_j/di}{R_j} \tag{17}$$

Consider the I-V characteristic of a diode

$$i = I_S \cdot \left[\exp\left(\frac{qv}{nkT}\right) - 1\right] \tag{18}$$

Where the reverse bias saturation current is denoted by $I_S$, the ideality factor $n$, the Boltzmann constant $k$. Then the current responsivity can be expressed as follows with equation (17) (18),

$$\mathfrak{R}_I = \frac{1}{2} \cdot \frac{q}{nkT} \tag{19}$$

From (19), we can conclude that the current responsivity $\mathfrak{R}_I$ does not depend on the junction resistance, but rather only on the process of fabrications and types of diode technology. The only intrinsic characteristic of diode that have an impact on the current responsivity is n, the diode's ideality factor. Thus, $\mathfrak{R}_I$ is inversely proportional to n and has a maximum value of 19.34 A/W at 300 K. This is the maximum current responsivity that any Schottky diode can reach at ambient temperature, thereby standing for an important limitation in the use of Schottky diodes for low-power energy harvesters [34]. Next, we can deduct the expression of RF-to-DC power conversion efficiency represented by the terms of current responsivity $\mathfrak{R}_I$ and junction resistance $R_j$ under ultra-low power region, where the junction resistance is considered to be constant and equal to $R_{j0}$.

The generated dc power that delivers into the dc load or the next stage of RF harvesting systems can be calculated,

$$P_{DC} = \frac{R_L}{(R_s + R_j + R_L)^2} \cdot v_{rect}^2 \tag{20}$$

Replacing $v_{rect}$ in (20) by the product of incident power $P_\omega$ and responsivity $\mathfrak{R}_v$ (15) (16),

$$P_{DC} = \frac{R_L \cdot P_\omega^2 \cdot \mathfrak{R}_i^2 \cdot R_j^2}{(R_s + R_j + R_L)^2} \tag{21}$$

Thus, using this model, the optimal $\eta_0 \cdot \eta_{DC-transfer}$ efficiency when the load connected to the diode is equal to $R_{j0}$ [12] is given by, assuming that $R_j \gg R_s$ and that the power that goes into the junction is low enough (-30dBm or below)

$$\eta_0 \cdot \eta_{DC-transfer} = \frac{P_{DC}}{P_\omega} = \frac{R_j \cdot \mathfrak{R}_i^2}{4} \cdot P_\omega \tag{22}$$

When the incident power is low, self-biasing current of the diode can be neglected and the diode can be viewed as zero-biasing when calculating the differential junction resistance $R_j$ and current responsivity $\Re_i$, denoted by $R_{j0}$ and $\Re_{i0}$.

### 4.1.4 Overall Efficiency

Above all, the overall efficiency of a rectifying diode can be calculated including all parts of efficiency contributions. However, it is difficult to integrate the matching efficiency into a generalized analytical model because this efficiency depends too much on the circuit technologies [12]. Thus, given a low power and ideal matching conditions ($\eta_M = 1$ and $R_j \gg R_s$), the optimum diode efficiency can be expressed

$$\frac{P_{DC}}{P_{RF}} = \eta_M \cdot \eta_p \cdot \eta_0 \cdot \eta_{DC-transfer}$$

$$= \left(\frac{\Re_i \cdot \sqrt{R_{j0}}}{2} \cdot \frac{1}{1 + \left(\omega \cdot C_j\right)^2 \cdot R_{j0} \cdot R_s}\right)^2 \cdot P_{in} \tag{23}$$

As a conclusion, at low power level, the power conversion efficiency is positively proportional to the power going into the junction $P_{in}$. And the trend of conversion efficiency of a diode can be discussed as follows considering the value of zero-bias resistance.

At low frequency, the term $\eta_0 \cdot \eta_{DC-transfer}$ dominates, which means that it is desirable to have the highest possible junction resistance. But in this case, matching loss cannot be neglected because the junction resistance is too much higher than the port impedance of the previous stage, typically an antenna.

At high frequency, the term $\eta_p$ dominates. A smaller junction resistance is then required.

Therefore, in the thesis it is important to choose a suitable Schottky diode for the design of rectifiers. For future works, the research topics may concentrate on the developments of the structure of rectifying devices [13], either on improvement of zeros bias current responsivity or ability to tune zero bias junction resistance.

Besides, the junction resistance $R_j$ is a function of the dc current flowing through the junction. The junction resistance will decrease as the voltage across the junction goes up. When the incident power is high enough, the resistance $R_j$ cannot be simply replaced by zero bias resistance $R_{j0}$ in calculations. The estimated efficiency from (23) can be further different with the value in reality for power levels higher than around -20 dBm. Plus, power will get into harmonics at these power levels due to the nonlinearity of rectifying diodes. Then the pre-assumption that no power goes into harmonics in mathematical analyses may not be correct and accurate. As a conclusion, the formula (23) is only applicable and accurate in ultra-low power region, especially below -30 dBm.

## 4.2 Rectifier Design and Simulation

### 4.2.1 Single Stage Half-wave Rectifier

In practice, a half-wave rectifier is firstly considered for low energy harvesting applications because of its simplicity. The previous work showed that an RF rectifier with a single stage of diode is more efficient in the ultra-low RF power domain than a diode ladder circuit [9]. Thus, a single stage half-wave rectifier is evaluated at first. Figure 13 shows a simple implementation of the half-wave rectifier, where a Π matching network is used to cancel the reflection of RF port. A basic LC low pass filter is attached to reject fundamental and high order harmonics.

According to the rectification model mentioned above, the power conversion efficiency of this rectifier can be estimated theoretically. In this structure, a low barrier zero-bias Schottky diode SMS-7630 is chosen. From datasheet [35], parameters are listed below:

a) The junction capacitance $C_j = 0.14$ pF
b) The internal series resistance $R_s = 20\ \Omega$
c) The zero bias current responsivity at 300 K (19)
$$\Re_I = \frac{1}{2} \cdot \frac{q}{nkT} = \frac{1}{2} \cdot \frac{1.602 \times 10^{-19}}{1.05 \cdot 1.381 \times 10^{-23} \cdot 300} = 18.41\ \mathrm{A/W}$$
d) The junction resistance $R_j \simeq 7\ k\Omega$ with the junction power of -30 dBm

Next, with the expression (23) of overall efficiency, excluding the loss of other passive components, an optimum efficiency is obtained.

$$\eta = \eta_M \cdot \left(\frac{\Re_i \cdot \sqrt{R_j}}{2} \cdot \frac{1}{1 + \left(\omega \cdot C_j\right)^2 \cdot R_j \cdot R_s}\right)^2 \cdot P_{in} \cdot 100\% \simeq 21.8\%$$

Another issue needed to be considered is that the equation here used to calculate the overall efficiency is deducted assuming that the current across the diode is a sinusoidal wave over the whole period, as mentioned in equation (10):

$$i_\omega(t) = M \cdot \cos(\omega t)$$

Therefore, when analyzing the case of a half-wave rectifier, the RF power in a half of the period is not collected. The final efficiency should be a half of the calculated value, i.e. 11% theoretically.

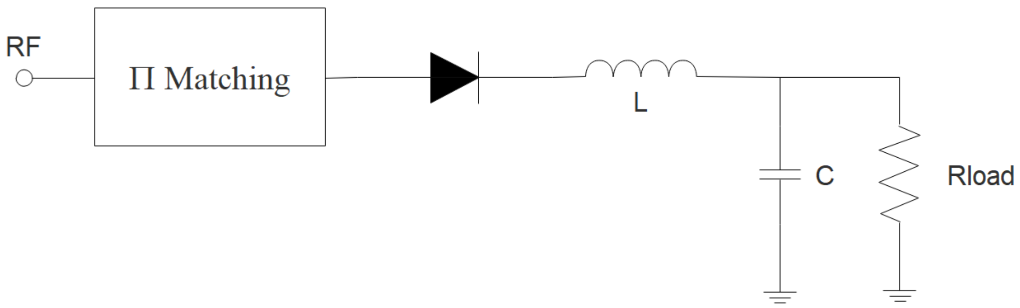


Figure 13. The schematic of a half wave rectifier with a single diode

For specific design, the impedance matching stage of the RF harvesting circuit is critical in order to deliver maximum power from the antenna to the rectifier circuit. However, matching network design is challenging since the rectifier diodes are nonlinear devices with complex impedance that vary with frequency, input power level and load resistance.

It is easy to understand that, for optimal matching performance, these parameters should be suitably determined prior to designing the matching network. For our RF rectifier, the operating frequency is from 2.4 to 2.5 GHz, a widely used band of multiple energy sources like Wi-Fi, Bluetooth, etc. Also, the anticipated input power is between -30 and -10 dBm, which is still much higher than the average value of ambient RF power but a reasonable power range used to demonstrate this design.

Furthermore, the load resistance for this design will be swept from 1kΩ to 10kΩ in order to track maximum power point (MPPT) of the rectifier.

The simulation of the half-wave rectifier is conducted in Microwave office. The center frequency is set to be 2.45 GHz. Figure 14 shows the matching reflections of center frequency 2.45 GHz on various input power and load points. The smith chart is expanded, where -10 dB and -20 dB contours are displayed. As we can see in the figure, S11 of most conditions, whose power is from -30 to -20 dBm and load from 1 kΩ to 10 kΩ, are constrained below -10 dB, an acceptable value for impedance matching.

Figure 15 is the simulated result of open-circuit voltage at diverse power levels, whose dc output voltage below -15 dBm is not high enough to overcome the cold start threshold of a boost converter used in next stage. Figure 16 shows the simulated power conversion efficiency of the designed half-wave rectifier. The maximum efficiency points at some power levels are marked on the figure. The optimal efficiency 12.7% at -30 dBm is corresponding to the estimated value 11% calculated previously.

One weakness of this topology is that only one half of the input waveform reaches the output assuming the condition of an ideal diode.

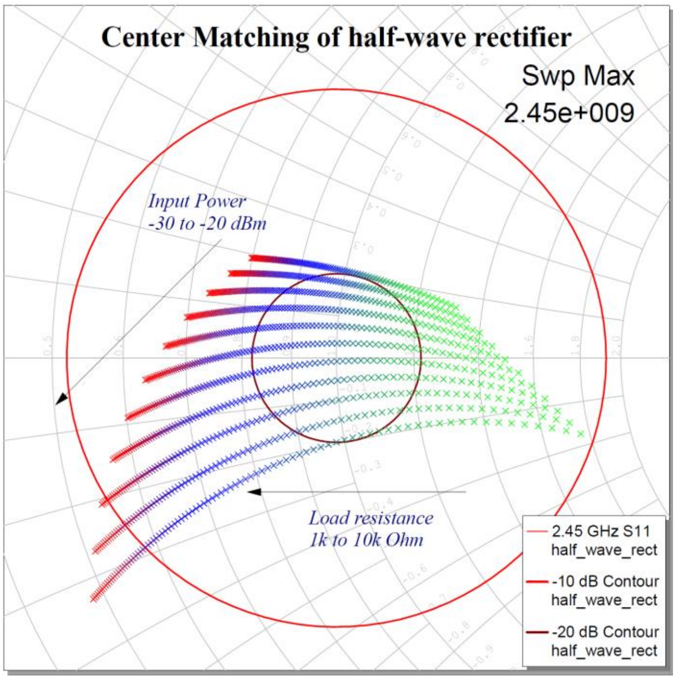


Figure 14. S11 at 2.45 GHz on various power and load points

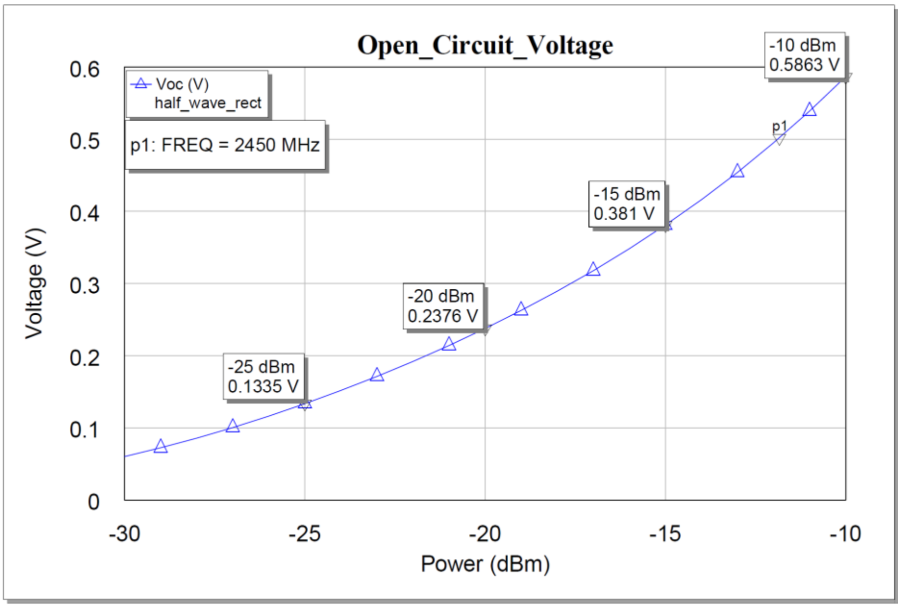


Figure 15. Open circuit voltage of the half wave rectifier against input RF power

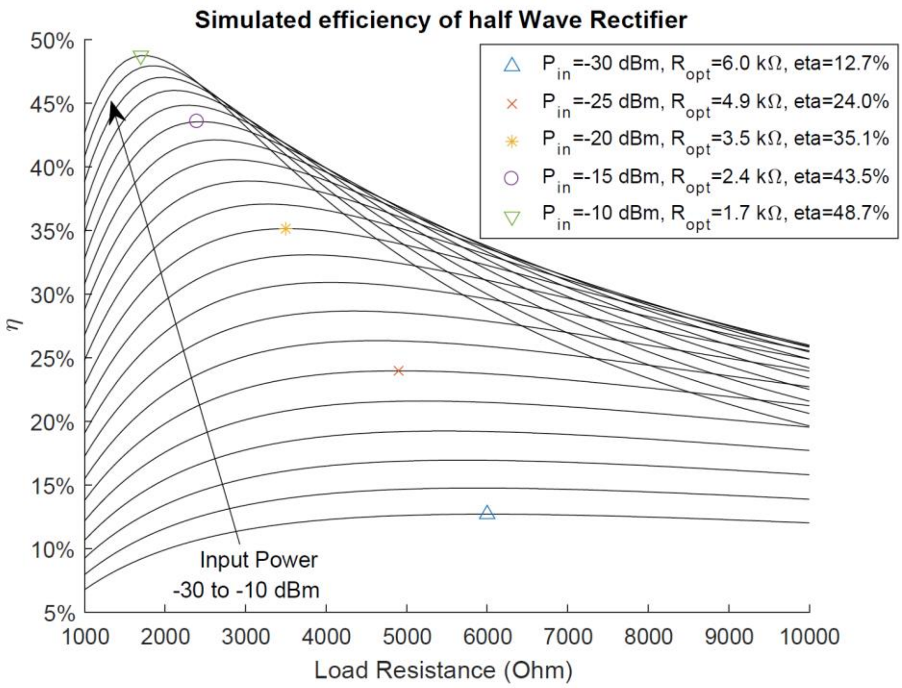


Figure 16. Simulated efficiency of the half wave rectifier

### 4.2.2 Modified Full-wave Rectifier

According to discussions above, a full-wave rectifier is then proposed. The modified structure of the differential full-wave rectifier is shown in Figure 17. In fact, the modified rectifier is composed of two single-stage full-wave rectifiers, whose polarity is opposite with each other. The resulting DC output is stacked up and easier to activate the boost converter. Four identical zero-bias Schottky diodes D1, D2, D3 and

D4 are used in the circuit, which are characterized as low-barrier, high-current-saturation and no additional biasing.

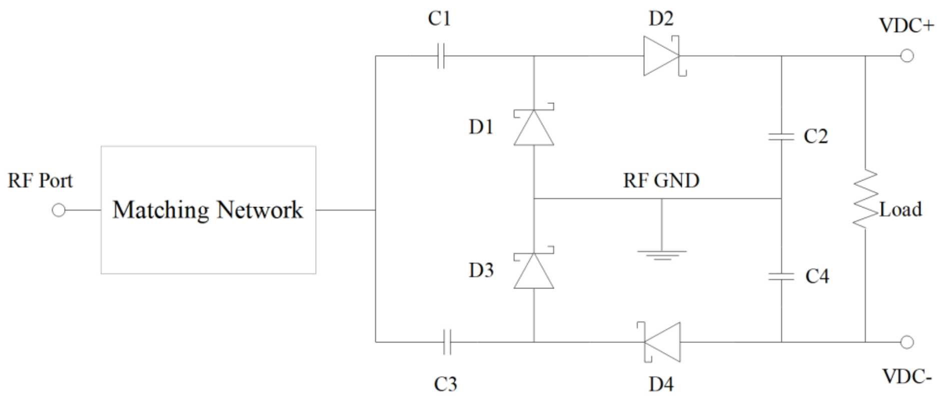


Figure 17. Structure of a differential full-wave rectifier

One of the most important drawbacks of this topology is the high impedance nodes at low power levels. On the one hand, the matching loss is pretty high because of the large gap between input and output matching impedance. On the other hand, the overall efficiency of the topology depends highly on substrate material considering medium loss of the substrate, which will be analyzed later in this chapter.

The operation of the modified full-wave rectifier can be explained considering either half side of the rectifier due to symmetry of the topology. For the upper side, when the polarity of input voltage is in negative cycle, where diode D1 is turned on and D2 is off, the energy is stored into capacitor C1 through the path of D1, as shown in Figure 18 (a). And when the polarity of excitation alters into positive cycle, where diode D1 is shut off and D2 is activated, the input energy is transferred and kept into capacitor C2 through the path of D2, as shown in Figure 18 (b). Meanwhile, the energy stored in capacitor C1 is also pumped to capacitor C2. Eventually, the energy stored in capacitor C2 supplies the dc power to the load, once the diode D2 is shut off in negative cycle. Due to the property of symmetry, the bottom side rectifier works similarly as the upper side one with opposite polarity.

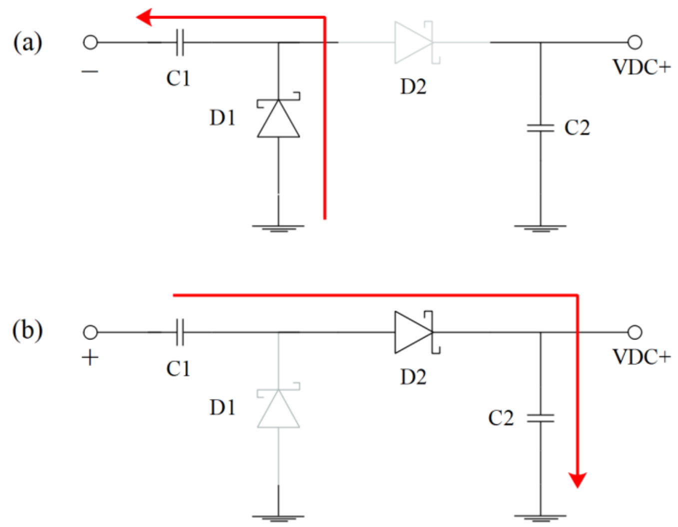


Figure 18. Operation of the upper side rectifier (a) negative cycle (b) positive cycle

As opposed to other rectifier circuits (such as Dickson or Villard), the version of rectifier is RF symmetric. As such, every rectifying diode is excited with the same input power ideally, if diodes are identical. In addition, this symmetry helps us reduce harmonics generated by the diodes (as even harmonics cancel each other).

It should be noticed that some other rectifier configurations that can operate near theoretical bounds of power extraction are available in the literature [36], [37]. But for our case, the modified full-wave rectifier are selected because it can be built using discrete components that is available commercially. Thus, the circuit is much easier to fabricate and evaluate.

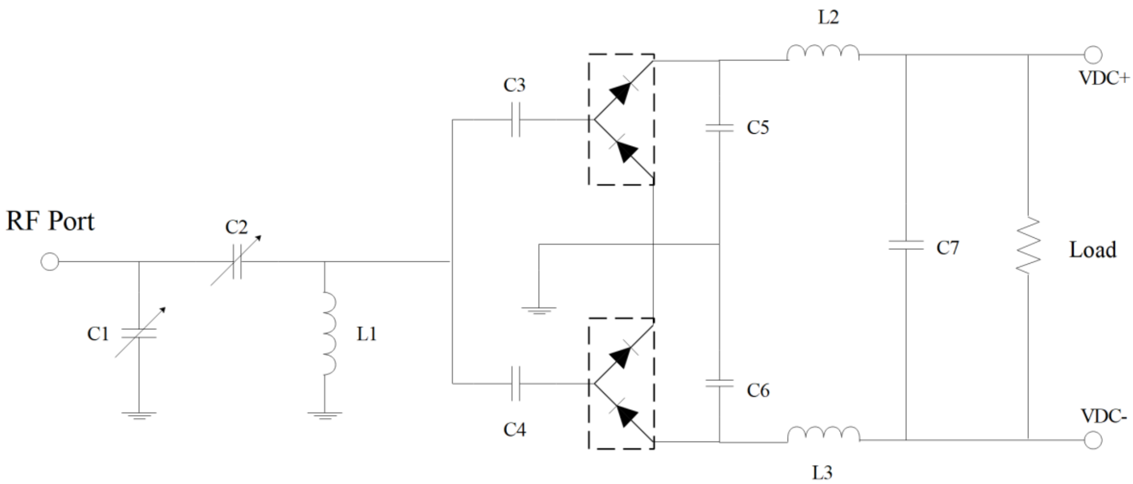


Figure 19. Schematic of the modified rectifier configuration

Figure 19 shows the configuration of the differential full-wave rectifier in detail. A tapped capacitor transformer is chosen for the matching network. All discrete components in the schematic are commercial available and their size and value are listed below in Table 3. Variable capacitors are used in the matching network to adjust reflection coefficient at desired 2.45 GHz frequency and power levels of excitations. And the circuit prototype is displayed in Figure 20.

Table 3. List of Components in fabricated rectifier

| Component | Manufacture | Part | Value | Q @ 2.45 GHz |
|---|---|---|---|---|
| C1 | Murata | Variable Cap | 1.4 - 3 pF | ~ 1 |
| C2 | Murata | Variable Cap | 1 - 2.5 pF | ~ 3.5 |
| C3, C4, C5, C6 | Murata | Ceramic Cap 0603 | 100 pF | ~8 |
| C7 | Murata | Ceramic Cap 0603 | 5000 pF | |
| L1 | Coilcraft | Air core spring 0906 | 1.65 nH | ~200 |
| L2, L3 | Coilcraft | Ceramic Ind 0603 | 33 nH | ~20 |
| Diode | Skyworks | SMS7630 SOT-23 | | |

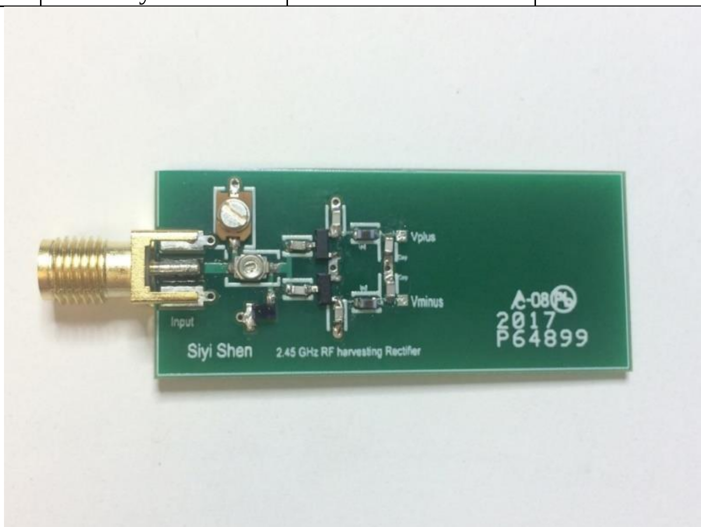


Figure 20. Fabricated rectifier circuit prototype

Simulations are conducted in Microwave office. The values of components are chosen to have the best matching (return loss less than -20 dB) for power from -30 to -20 dBm and optimal load resistance. Figure 21 shows the impedance matching at center frequency 2.45 GHz with diverse power and load resistance points. The Smith chart is again expand, where -10 dB and -20 dB contours are displayed. The return loss of most of conditions are limited below -10 dB.

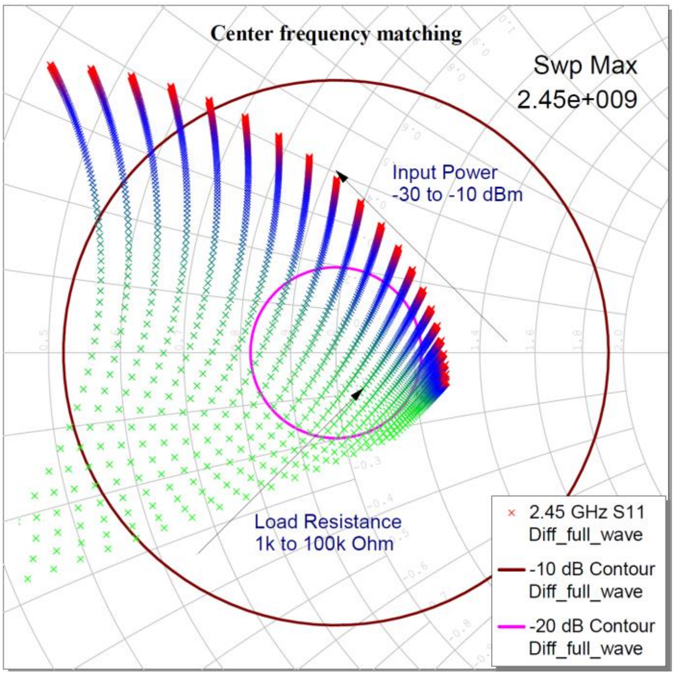


Figure 21. S11 of 2.45 GHz on various power and load points

Figure 22 shows the open circuit voltage of the modified rectifier at different input power levels. Figure 23 is the simulated efficiency of the rectifier, where maximum efficiency points are marked on the figure. The efficiency values of this rectifier are lower than that of the half-wave rectifier, since series resistance among diodes is increased, which results from the increased number of Schottky diodes. This can be foreseen in the mathematical analyses above.

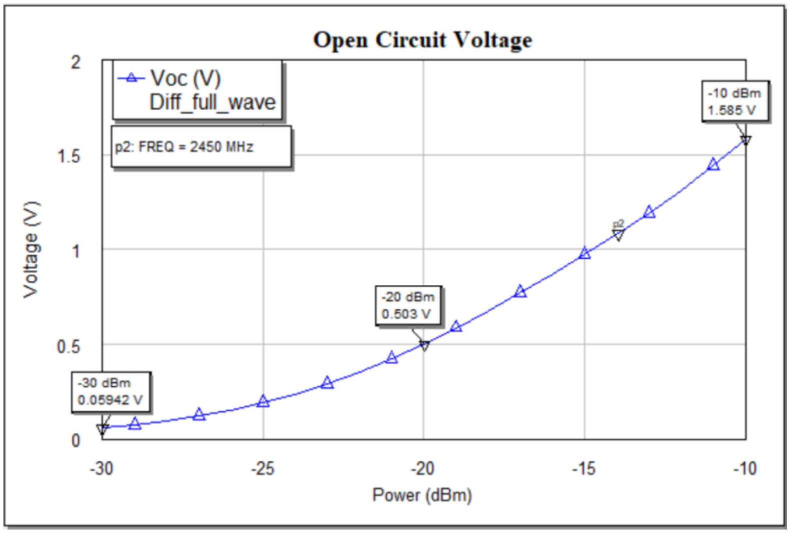


Figure 22. Open circuit voltage against Input RF power

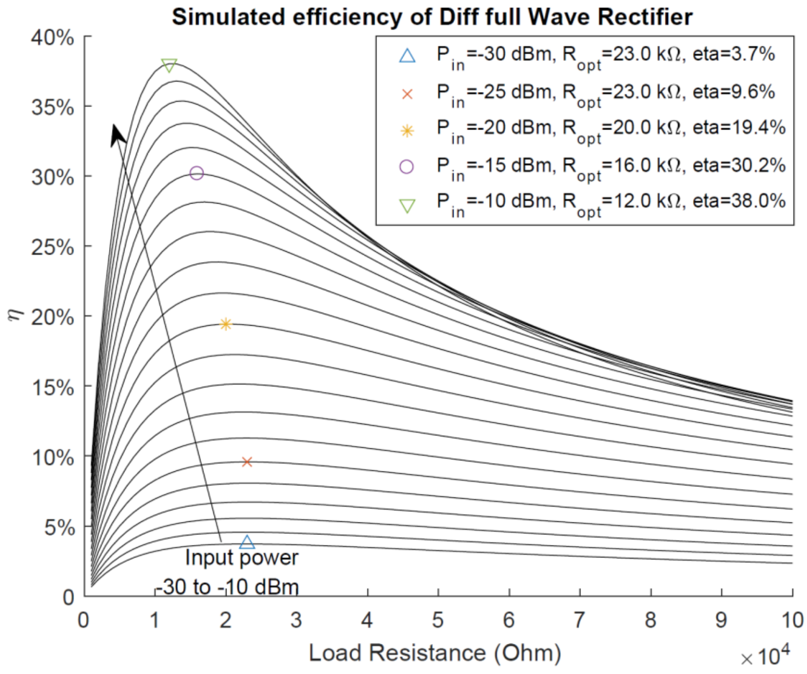


Figure 23. Simulated efficiency of the full-wave rectifier for various power and load resistance

Figure 24 shows the measured S11 at 2.45 GHz. Similarly, the Smith chart is expanded, where -10 dB and -20 dB contours are displayed. The distribution is not identical to that of simulations but reasonable considering parasitic elements from the fabrication and discrete components. Figure 25 is measured open-circuit voltage of the rectifier, where the results are slightly lower than that in simulations due to some parasitic components. Figure 26 presents the plot showing measured efficiency of the rectifier, where maximum efficiency points are clearly marked on the graph every 5 dB interval. The load resistance is varied with a potentiometer connected with two copper lines.

As we expected, the measurements shows the similar trend as the simulations that optimal load resistance decreases as the input power excitation goes up from -30 to -10 dBm. The reason for the tendency is related to junction resistance of rectifying diodes, whose value change can be foreseen in diodes' I-V characteristics. It should be noticed that a series of abnormal data points measured at a load of 22kΩ may result from the fluctuation of waveform generated by the RF signal generator. Another possible reason is a small deviation of the tuned value that appears when manipulating the potentiometer.

On the other hand, the values of measured efficiency are much lower than what we anticipated from simulations. Analyses are carried out as follows in detail and some possible reasons are presented.

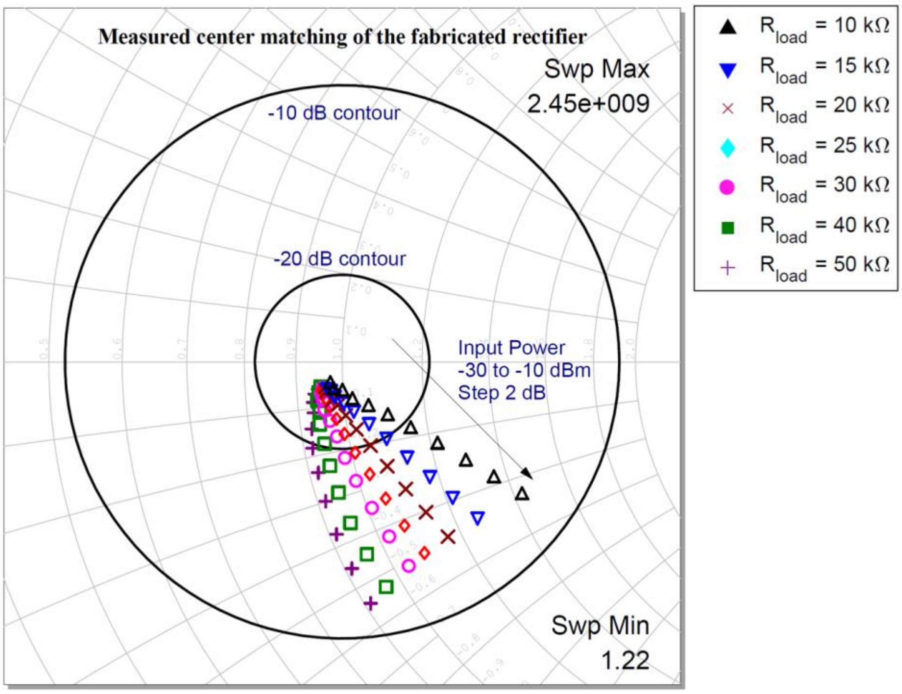


Figure 24. Measured S11 at 2.45 GHz for diverse input power and load resistance

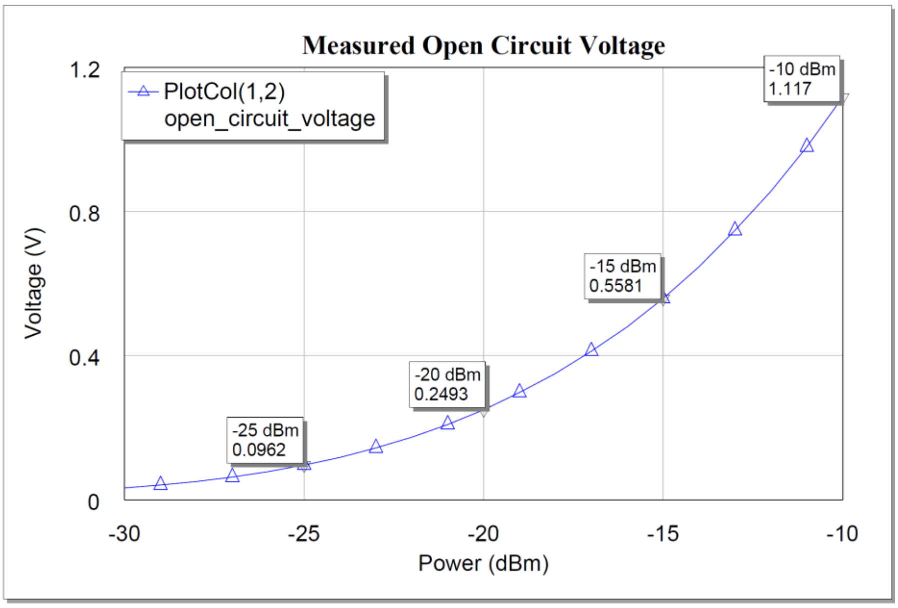


Figure 25. Meausred open circuit voltage of the fabricated rectifier

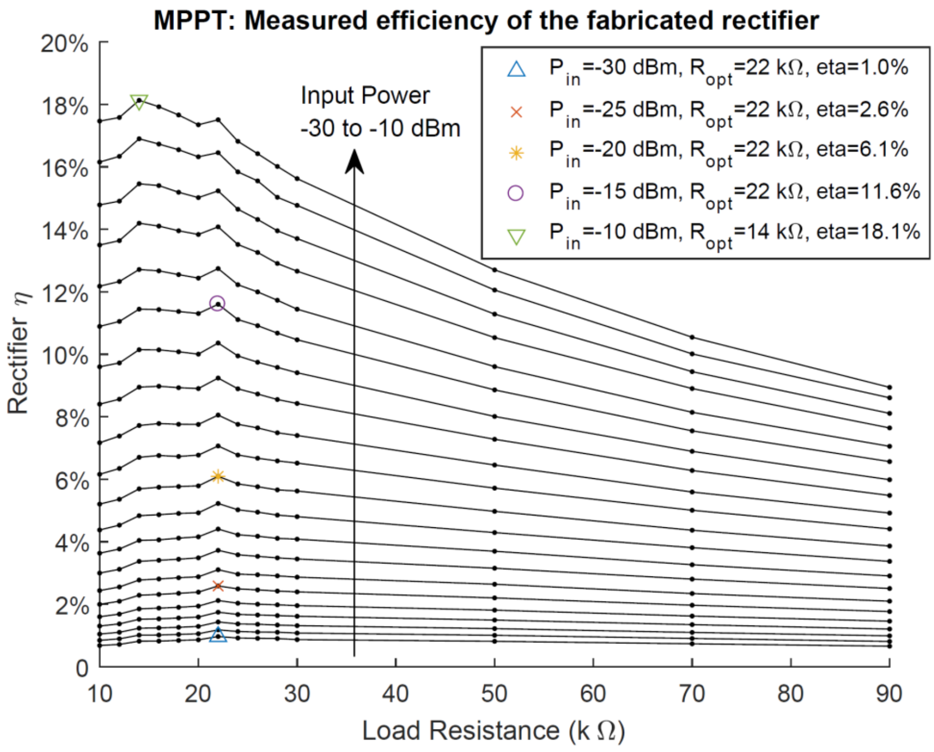


Figure 26. Measured efficiency of the modified rectifier

Theoretical analyses are presented below to discuss the reasons that account for the discrepancy between simulated and measured efficiency of the modified RF rectifier.

First of all, loss in medium is a critical factor for the difference between simulations and measurements. In fact, the substrate material of PCB used for the rectifier is FR4, whose dielectric tangent loss is approximately 0.02. At the desired 2.4 – 2.5 GHz frequency range, the resulting dielectric conductivity then cannot be neglected, degrading the performance of the entire circuit. With an insight inspection, it is understandable that the moderate substrate resistance influences the quality factor of impedance matching circuit and divides the current flow that is delivered into the system load of the rectifier, dissipating a portion of energy harvested from an antenna or a dedicated RF signal generator.

In general, the complex permittivity is defined as [38]:

$$\varepsilon = \varepsilon' + i\frac{\sigma}{\omega} \tag{24}$$

where $\sigma$ is the conductivity of a medium, $\varepsilon'$ is the absolute permittivity.

The tangent loss of dielectric is expressed as

$$tan\delta = \frac{\varepsilon''}{\varepsilon'} = \frac{\sigma}{\omega\varepsilon'} \tag{25}$$

Thus, the dielectric conductivity of the medium is then calculated:

$$\sigma = \omega\varepsilon' \cdot tan\delta = \omega\varepsilon_0\varepsilon_r \cdot tan\delta$$

In this case, the dielectric conductivity of FR4 material at center frequency 2.45 GHz can be estimated as follows:

$$\sigma = \omega\varepsilon_0\varepsilon_r \cdot tan\delta$$

$$= 2\pi \times 2.45 \times 10^9 \times 8.854 \times 10^{-12} \times 4.4 \times 0.02 = 0.012\ \mathrm{S/m}$$

Thus, substrate resistance can be estimated by the equation (26), where *H* is the thickness of substrate in PCB process and *A* is the copper area of certain nodes on layout pattern.

$$R_{sub} = \frac{H}{\sigma A} \tag{26}$$

As a conclusion, Table 4 presents estimated areas of connection node in layout pattern (shown in Figure 28) of the rectifier in the left column and calculated substrate resistances to the ground plane in the right list. $\mathrm{H} = 62$ mil is used for calculations below.

Table 4. Estimated node areas and substrate resistance

| Node | copper area ($mm^2$) | Substrate Resistance(kΩ) |
|---|---|---|
| A | 11.36 | 11.55 |
| B | 7.14 | 18.38 |
| C | 0.96 | 137.24 |
| D | 1.82 | 72.15 |
| E | 2.34 | 56.06 |

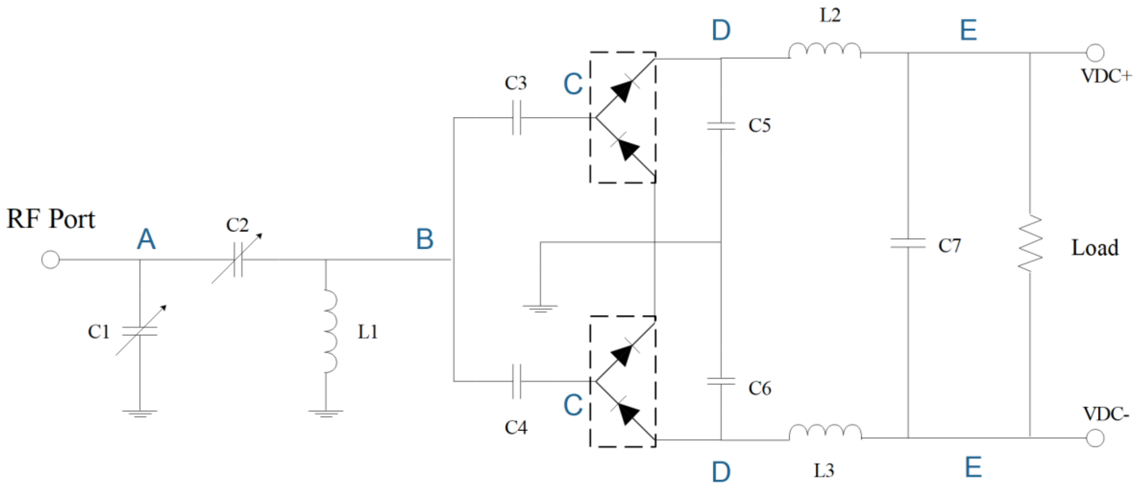


Figure 27. Nodes denotation of the full-wave rectifier

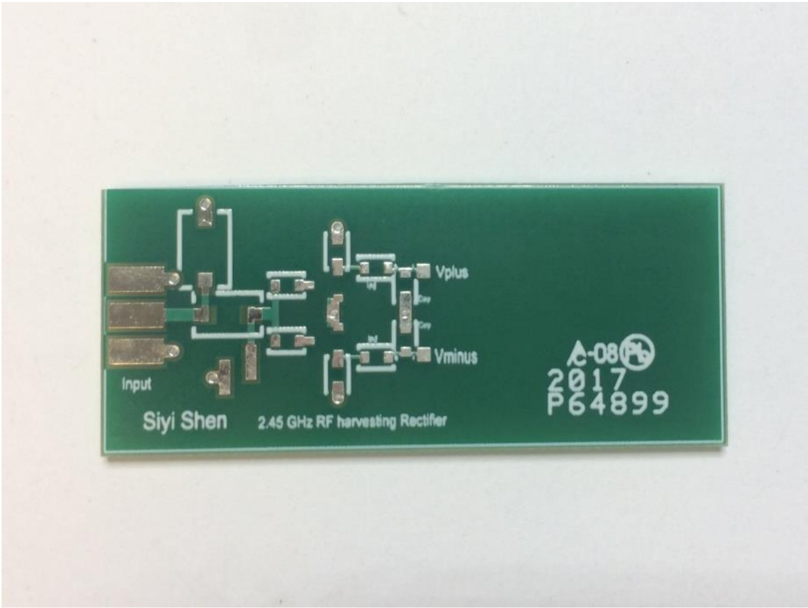


Figure 28. Layout pattern of the fabricated rectifier

Figure 29 and Figure 30 are simulated open circuit voltage and power conversion efficiency of the full-wave rectifier after considering substrate loss in the simulation, respectively. Based on the simulation results, we can conclude that the substrate loss has great impact on the overall performance of the rectifier as expected, including output open circuit voltage and power conversion efficiency, at all levels of power excitation.

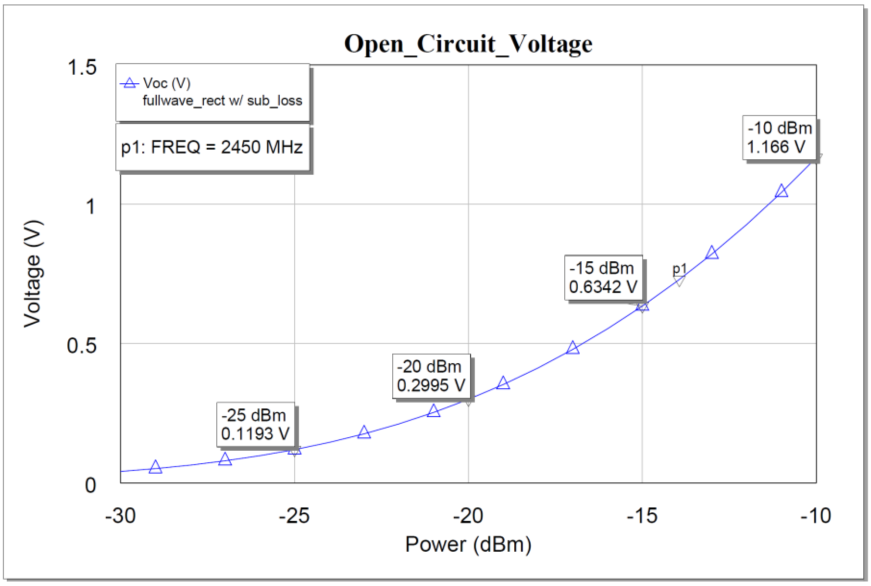


Figure 29. Open circuit voltage of the rectifier considering substrate loss

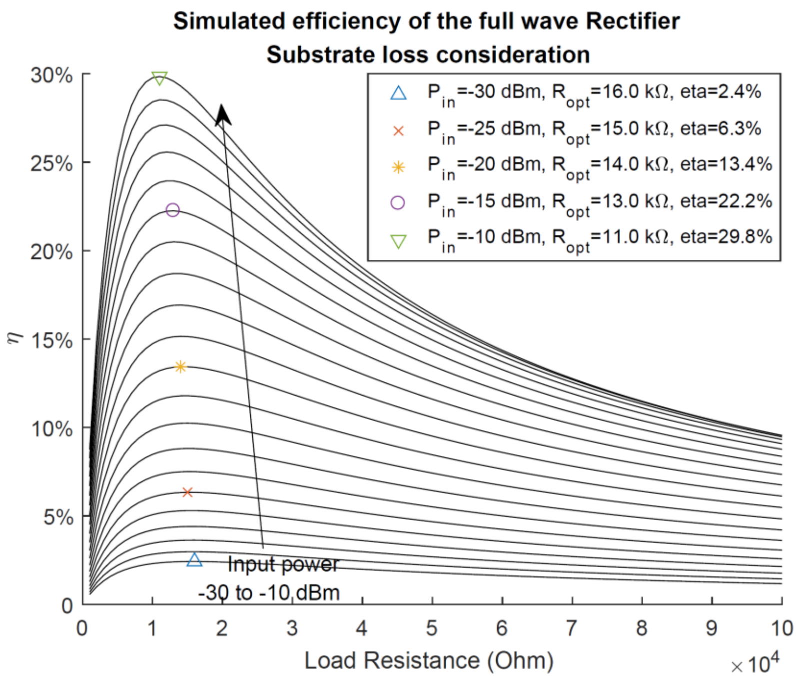


Figure 30. Simulated efficiency of the rectifier considering substrate loss

Secondly, parasitic loss of discrete components, including rectifying diodes and LC elements on the rectifier, can have negative impact on the overall efficiency of the rectifier. In this design, although it is much convenient to use two tunable capacitors to match the desired center frequency of the rectifier, the quality factor of these capacitors can be as low as one at 2.45 GHz according to the graphs provided by the manufacturer. And the estimated series resistance of the tunable capacitors at 2.45 GHz is around several Ohm. The quality factors of each component in this design are listed in Table 3. After replacing all components on the schematic by models that are offered by manufacturers (Murata, Coilcraft), and inserting components of the calculated parasitic resistance into the schematic, a more accurate result of the rectifier efficiency is extracted from simulation, combined with the consideration of lossy substrate, as shown in Figure 31. This result is much closer to what we have in measurement.

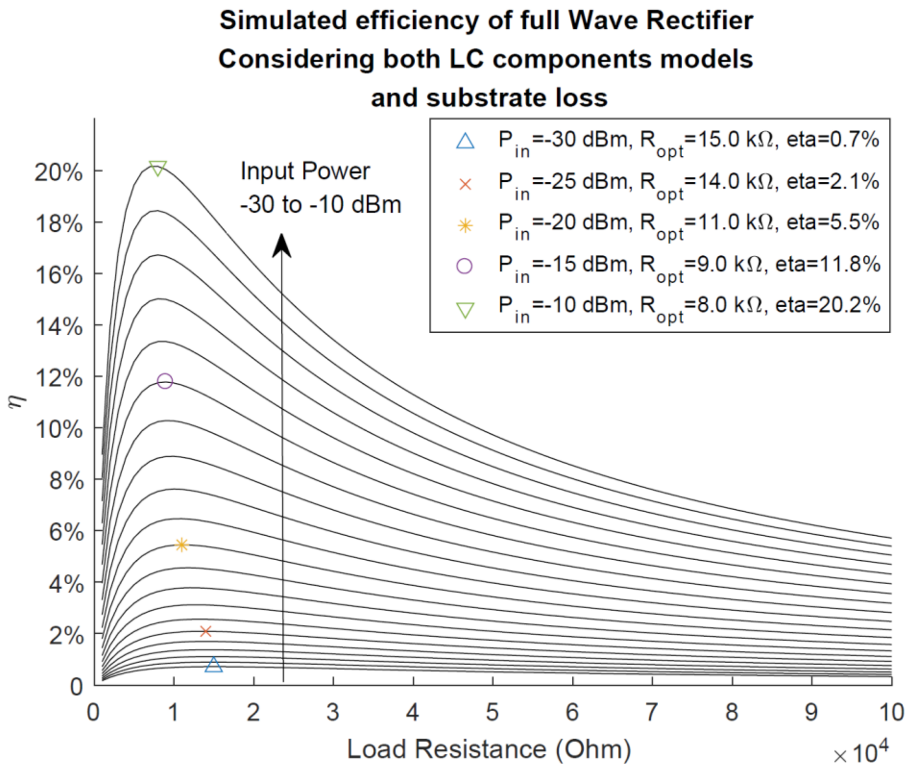


Figure 31. Simulated efficiency of the rectifier considering both substrate loss and LC components models

Illustrated in Figure 32 is the comparison between the results of power efficiency from measurement and simulation with incident power levels of -30, -20 and -10 dBm. Obviously, the optimal load resistances at each power levels from simulations are much lower than that from measurement. Generally, the measured curves greatly fit the curves that are translated from dash-dot lines. An important factor is that the expected values of load resistance is far higher than the real values implemented during measurements. Two key features can be the internal resistance inserted from the multi-meter and the real substrate resistance that is much lower than estimated ones in Table 4. The other possible reason may be the inaccurate models for tunable capacitors in simulation. Since no parasitic models offered from online datasheets, only estimated parasitic components are added in simulation as the influence of discrete components. Thus, the models may explain the reasons for efficiency degradation rather than represent the accurate results.

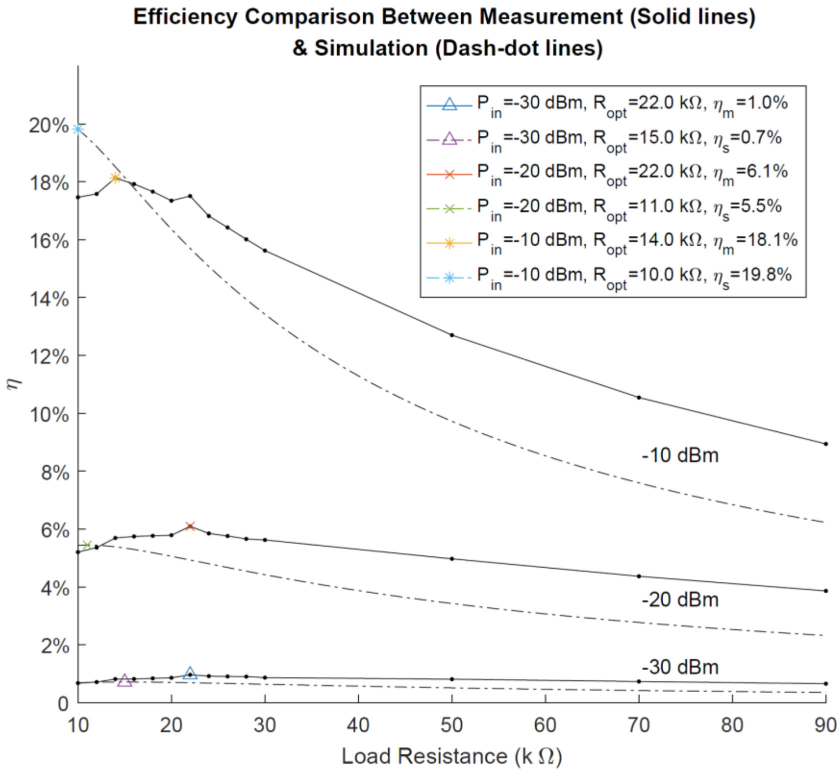


Figure 32. Comparison of the efficiency of the rectifier between simulation and measurement

Besides, another possible reason explaining for the difference is the inevitable diversity of discrete components that comes from fabrication process. Among the impact of those elements, the most important one results from the diversity of rectifying diodes, in which reverse saturation current $I_s$ and forward built-in voltage $V_F$ can vary. A previous work [39] published by the team of Prof. Wu have discussions about the impact of reverse saturation current $I_s$ on RF-to-DC power conversion efficiency of a rectifier with a single rectifying diode. In their paper, the RF power dissipated in the short circuited stub and in the series matching network transmission line, as a function of $I_s$ are given, as shown in Figure 33.

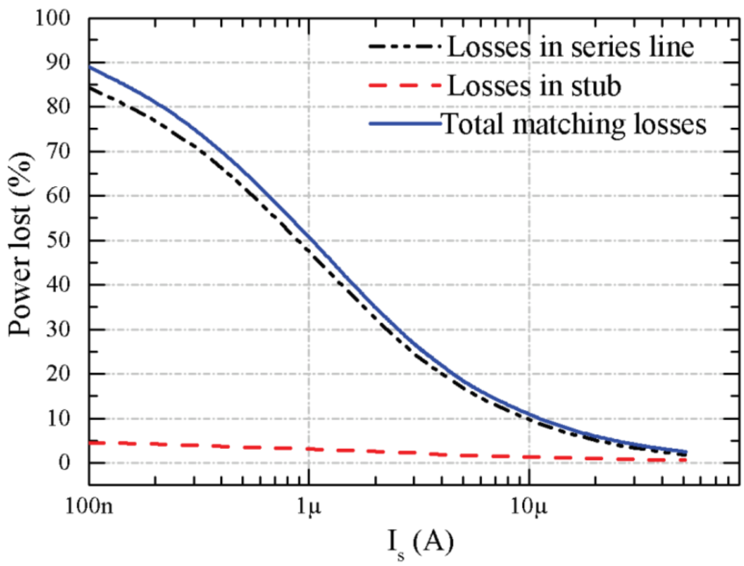


Figure 33. Power dissipated in the matching network as a function of the diode's saturation current. [39]

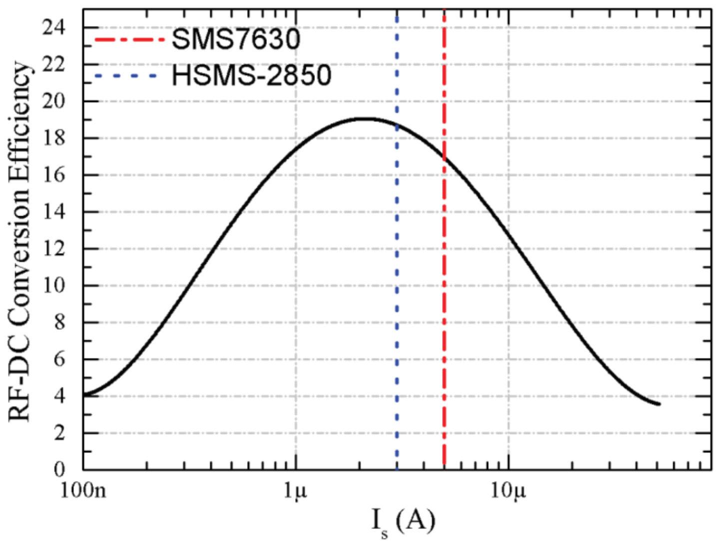


Figure 34. Total RF to DC power conversion efficiency as a function of the diode's zero-bias resistance. Input power is -30 dBm at 1.95 GHz. [39]

And the total harvesting efficiency indicating the saturation current of both SMS7630 and HSMS2850 is also presented in the paper, shown in Figure 34. It is obvious to conclude that the difference of saturation current can have great impact on the overall power efficiency.

# Chapter 5. Boost converter module

In this chapter, the integrated device for ultra-low energy harvesting bq25570 from *Texas Instruments* is described. And for convenience and the limitation of fabrication conditions, a commercial bq25570EVM-206 evaluation board is used for DC-DC voltage conversion and power storage and management. Node connections of the evaluation module are shown in figures and specified below. A supercapacitor with a reduced leak current of 10nA is attached to the output of the module. Then is measured the power conversion efficiency of Boost converter at different power levels with two source-meters.

## 5.1 Bq25570 Programmable Integrated Nano-power Boost Charger IC

The bq25570 device is specifically designed to efficiently extract micro-watts (μW) to mill-watts (mW) of power generated from a variety of high output impedance DC sources like photovoltaic (solar) or thermal electric generators (TEG) without collapsing those sources [40]. In ambient RF energy harvesting, the power received from the RF-to-DC rectifier is typically on the order of micro-watts. Besides, according to the measurements above, the voltage extracted to the boost converter is relatively low. In steady state condition, the bq25570 ensures continuous energy harvesting from an input voltage as low as 100mV, which is suitable for this application.

As for the power management part, the battery management features ensure that a rechargeable battery or other storage devices are not overcharged by this extracted power, with voltage boosted, or depleted beyond safe limits by a system load [40]. In addition to the highly efficient boosting charger, the bq25570 integrates a highly efficient, nano-power buck converter for providing a second power rail to systems such as wireless sensor networks (WSN) which have stringent power and operational demands. The buck converter as a voltage regulator at output is vital to set reasonable threshold voltage limitations for storage devices with different maximum voltage.

One of the most beneficial features of this device is that a controller for maximum power point tracking (MPPT) is contained inside the IC [40]. MPPT is essential in energy harvesting applications in order to maximize the power extracted from an energy harvester source.

The MPPT controller modulates the input impedance of the main boost charger by regulating the charger's input voltage, as sensed by the VIN_DC pin, to the sampled reference voltage, as stored on the VREF_SAMP pin. The MPPT circuit obtains a new reference voltage every 16 s by periodically disabling the charger for a very short duration and sampling a fraction of the open-circuit voltage (VOC) [40]. For RF energy harvesters, the maximum power point is typically 40%-50%. In the evaluation board we use, two values of 80% and 50% have already been set up for typically applications. The MPPT regulation point can be internally set by connecting VOC_SAMP to either VSTOR or GND.

### 5.2 Efficiency Measurement

The measurement setup is illustrated in Figure 35. The specific equipment used for the measurement results is presented in Figure 36 and Figure 37. The detailed setup is described below:

1) Node VIN_DC was connected to a Keithley 2400 source-meter configured as a voltage source with current compliance (Cmpl) set to the input current of the boost converter. The voltage source serves as the function of the RF-to-DC rectifier. In this measurement, the open circuit voltage is set to be 0.5 V and 1.1 V, a typical dc output voltage receiving from the designed rectifier.

2) Node VOUT was connected to a Keithley 2401 source-meter configured as a voltage source set to the VOUT voltage. The voltage source is regarded as a rechargeable battery at the pin VSTOR, whose open circuit voltage is tuned to be a general operating voltage of the storage device MS920SE 2.6 V. The current getting into the source-meter (displayed as a negative value) is the output current of the charger.

Conditions of the measurement are summarized as follows:

1) Input: Keithley 2400, $V_{src1}$=0.5 V / 1.1V, $I_{cmpl}$ varies from 30 to 100 $\mu A$ with a step of 5 $\mu A$.
2) Output: Keithley 2401, $V_{src2} = 2.6V$, $I_{out}$ is measured.

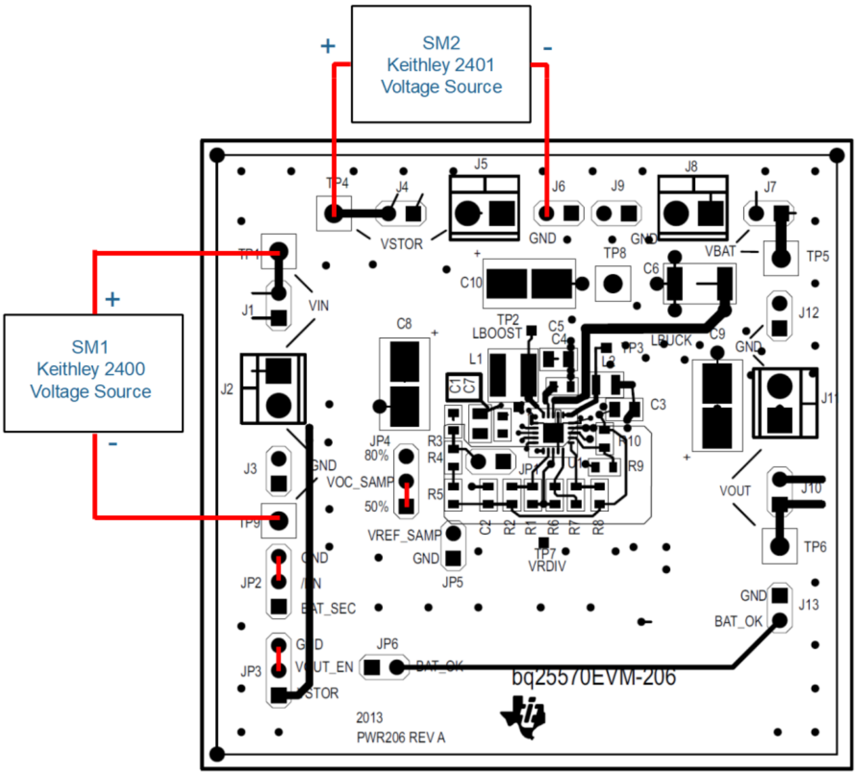


Figure 35. Measurement setup of the boost converter evaluation module


Figure 36. Two source-meters used in measurements

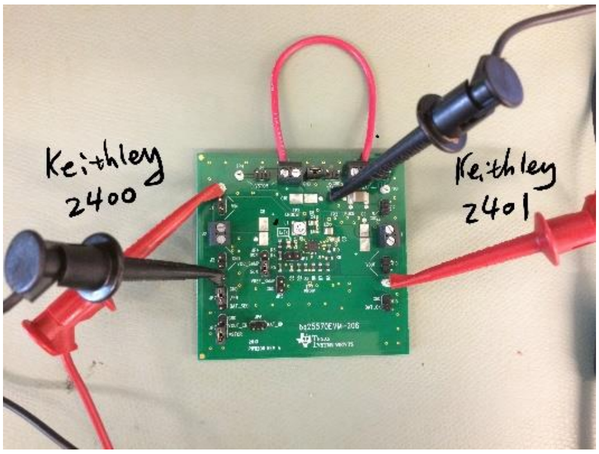


Figure 37. The Boost converter module connected to source-meters

In Table 5, the efficiency is obtained from the expression below:

$$\eta = \frac{|I_{out}| \cdot V_{src2}}{P_{in}}$$

Table 5. Measurement of the input voltage and output current of boost converter module

| $I_{in}$ (μA) | Voc = 0.5 V, Vout = 2.6 V | | | Voc = 1.1 V, Vout = 2.6 V | | |
|---|---|---|---|---|---|---|
| | Measured $V_{in}$ (V) | $I_{out}$ (μA) | $\eta$ % | Measured $V_{in}$ (V) | $I_{out}$ (μA) | $\eta$ % |
| 30 | 0.235 | -1.41 | 52.0 | 0.539 | -4.54 | 73.0 |
| 35 | 0.236 | -1.76 | 55.4 | 0.539 | -5.46 | 75.3 |
| 40 | 0.235 | -2.08 | 57.5 | 0.539 | -6.29 | 75.9 |
| 45 | 0.235 | -2.42 | 59.5 | 0.540 | -7.22 | 77.3 |
| 50 | 0.235 | -2.77 | 61.3 | 0.540 | -8.09 | 77.9 |
| 55 | 0.235 | -3.11 | 62.6 | 0.541 | -8.96 | 78.3 |
| 60 | 0.235 | -3.47 | 64.0 | 0.541 | -9.85 | 78.9 |
| 65 | 0.236 | -3.81 | 64.6 | 0.540 | -10.73 | 79.5 |
| 70 | 0.235 | -4.14 | 65.4 | 0.542 | -11.61 | 79.6 |
| 75 | 0.236 | -4.50 | 66.1 | 0.541 | -12.46 | 79.8 |
| 80 | 0.235 | -4.84 | 66.9 | 0.541 | -13.36 | 80.3 |
| 85 | 0.236 | -5.17 | 67.0 | 0.541 | -14.25 | 80.6 |
| 90 | 0.236 | -5.54 | 67.8 | 0.540 | -15.14 | 81.0 |
| 95 | 0.236 | -5.86 | 68.0 | 0.539 | -15.96 | 81.0 |
| 100 | 0.236 | -6.21 | 68.4 | 0.539 | -16.84 | 81.2 |

The measured input voltage is approximately a half of voltage provided by a source-meter. And voltage is refreshed every several seconds. This means that the boost converter works well as what we expected.

Based on measurements, as we can see in Table 5 and Figure 38, the overall DC-DC efficiency of the boost converter module is over 50 percent, which is outstanding at low power working region among commercial products for applications of low power DC-DC conversion and energy management. Especially, when the voltage of the input source-meter is set to 1.1 V that is approximately the open circuit voltage of the designed rectifier in the thesis, the boost converter can have an efficiency at least 70% with a provided power of around 15 micro-watts.

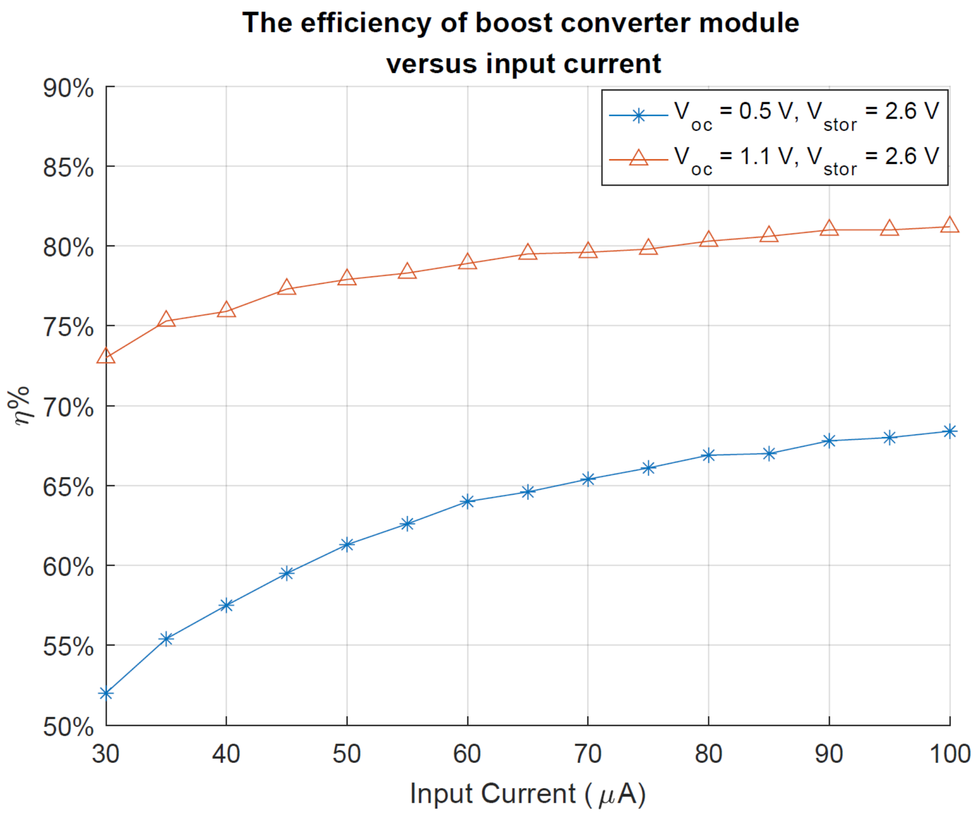


Figure 38. Measured DC-DC conversion efficiency of boost converter versus input current

# Chapter 6. Experimental demonstration of the entire energy harvester

## 6.1 Demonstration with RF signal generator

The entire RF energy harvester including an RF signal generator, the fabricated rectifier, the boost converter evaluation board and a supercapacitor/battery is firstly set up together to test its performance with desired power excitation, which is shown in Figure 39 and Figure 40.

Based on datasheet of bq25570 [40], the minimum cold-start input power of the boost converter is 15 µW and the minimum input voltage for cold start is 330mV. Thus, the boost converter module cannot be activated to work until the DC output from the RF rectifier reaches these two thresholds. So for our case, the entire power harvester attaching a 7.5mF supercapacitor is excited with -10 dBm RF signal. The input and output voltage of the boost converter are measured with two multimeters, as shown in Figure 39 and Figure 40. The transient voltage of the supercapacitor is illustrated in Figure 41. First, the input voltage of the boost converter keeps in a voltage of 334mV for 104s after turning on the -10 dBm RF signal generator, which means the overall system is on the state of cold starting. After that, the input voltage constantly stays at around a half of the open circuit voltage of the fabricated rectifier with incident power of -10 dBm and is refreshed every 15 seconds. Thus, the voltage of supercapacitor is recorded with an interval of 15 second.

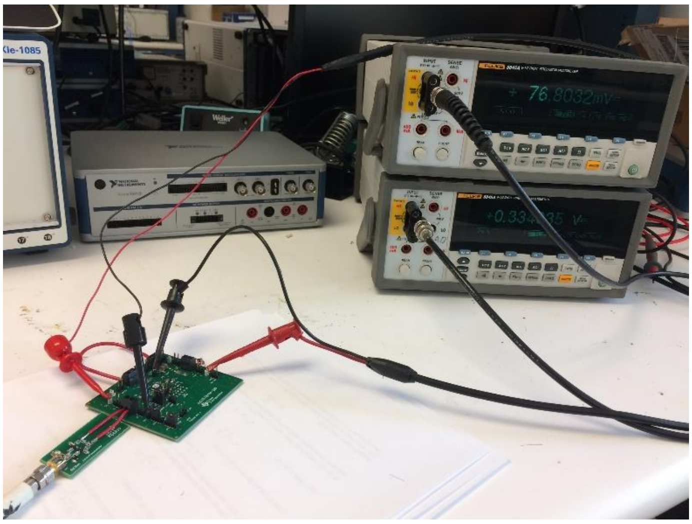

Figure 39. RF power harvesting system at the state of cold starting

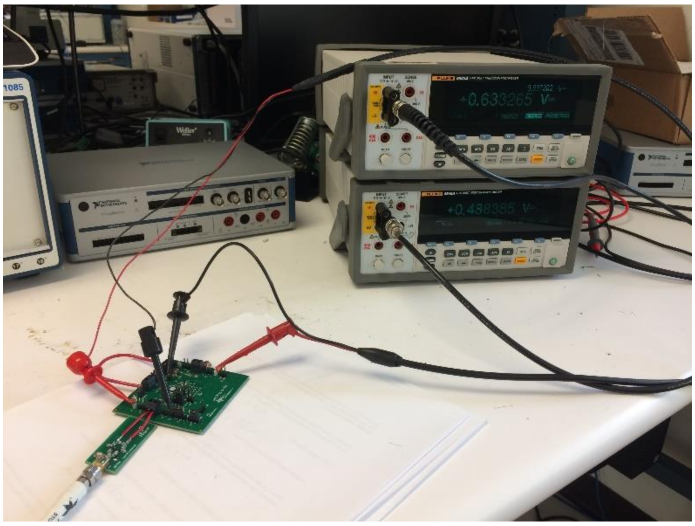


Figure 40 RF power harvesting system at steady state of charging a supercapacitor

According to the result in Figure 41, the overall collected energy over time can be estimated with formula below

$$E_{store} = \frac{1}{2} \cdot C \cdot \left(V_2{}^2 - V_1{}^2\right) = \frac{1}{2} \cdot 7.5 \times 10^{-3} \cdot (1.792^2 - 0.524^2)$$
$$= 1.1 \times 10^{-2} \text{ Joule}$$

Then, the average DC power flows into the supercapacitor during the period of charging is obtained as follows:

$$P_{avg} = \frac{E_{store}}{t} = 5.174 \ \mu\text{W}$$

Thus, the overall efficiency can be calculated with input power of -10 dBm or 100 μW,

$$\eta = \frac{P_{avg}}{Pin} = 5.174 \ \%$$

Above all, the efficiency of the entire system is about 5.17%.

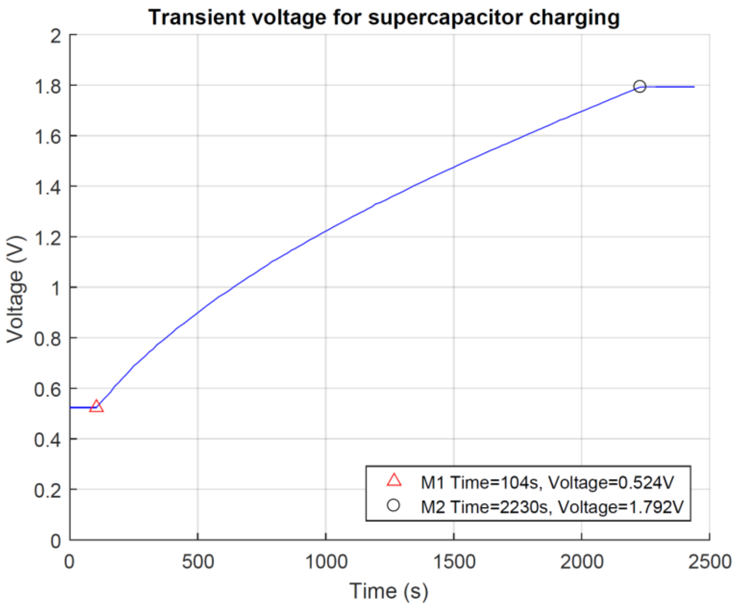


Figure 41. Transient voltage of supercapacitor charging with -10 dBm

### 6.2 Comparisons and conclusions

The comparison of this work to the other available power harvesters is shown in Table 6. At 2.45 GHz, the power harvester presented in this thesis performs with an average efficiency of 5.17% at -10 dBm when charging a supercapacitor by connecting it to the output of PFM buck converter, the 1.8 V pin V_OUT. When charging a supercapacitor, the RF sensitivity of our power harvester is around -10 dBm at the beginning due to the cold-start energy requirements of the boost converter. But once the pin VSTOR reach around 1.8 V, the system can continue to harvest energy down to -18 dBm and the PFM buck converter can work to output 1.8 V at the pin V_OUT. Thus, the barrier of cold-start condition required for activating the boost converter can be eliminated and the sensitivity of the system can be down to around -18 dBm where the input voltage is around 120 mV when a rechargeable battery with a voltage higher than 1.8 V is attached on VSTOR. Based on separate measurements in Chapter 4 & 5, the estimated efficiency of battery charging can reach around 13%. But the measured efficiency of battery charging is not available due to the lack of suitable battery to determine power charging efficiency.

As a comparison, the work from [41] is also implemented with discrete components on FR-4. This work has the second best sensitivity (including battery charging in this work) because the combination of a single Schottky diode and an ultra-low input voltage Seiko charge-pump IC is used to deliver power into a microcontroller platform. And the rectifier is matched to -12 dBm on average, which maximizes the efficiency of the rectifier at this power level. Thus, when incident power is -10 dBm, the measured efficiency of the system is slightly high than what we have in the thesis where the rectifier is optimized at a low power level around -30 dBm.

As for the work presented in [42], the technology is a two-metal two-poly 0.5-μm digital CMOS process. The overall efficiency is decreased due to the use of Silicon–Titanium Schottky diodes with the relatively high series resistance of 300 Ω. But compared with our RF rectifier, the impact of substrate loss is eliminated.

In addition, the work shown in [43] utilizes a step-up transformer inserted between the antenna and voltage multiplier of passive wireless microsystems to perform both power matching and voltage amplification prior to rectification to improve the efficiency of overall power harvesting microsystems. The technology implemented is TSMC 0.18-μm 1.8-V six-metal CMOS technology with thick-metal options. The proposed power matching technique shows a better performance than LC matching. But the structure of the implemented rectifier is an original voltage multiplier that is less efficient than the topology in this thesis.

Table 6. Performance comparison of power harvesters

| References | This work | [41] | [42] | [43] |
|---|---|---|---|---|
| Frequency | 2.45 GHz | 2.45 GHz | 2.45 GHz | 2.45 GHz (Simulation) 3.85 GHz (fabrication) |
| Sensitivity (dBm) | -10 (Output) -18 (Battery) | -15.6 | -13.5 | -12.0 |
| Maximum output voltage (V) | 1.8 (Output) 4.2 (Battery) | 2 | 1.5 | 1 |
| System efficiency | 5.17% @ -10dBm (Output), 13% (est.) @ -10 dBm (Battery) | 7.27% @ -10 dBm 6.5% @ -12 dBm 4.6% @ -14 dBm 2.7% @ -15.6 dBm | 5% @ -13.5 dBm | 2.7% @ -12 dBm |
| Fabrication process | Discrete components on FR-4 | Discrete components on FR-4 | 0.5 μm CMOS, Schottky diodes | 0.18μm CMOS |

## 6.3 Improvements and future works

### PCB Substrate

As we discussed above, for our modified full-wave rectifier, the FR-4 substrate loss is not negligible and has a great impact on the performance due to high impedance nodes at low power levels on the rectifier. Thus, in order to improve the power conversion efficiency, substrate materials with lower electrical loss and lower relative permittivity, such as RO4000 series, RT/duroid series, will be selected to demonstrate the modified rectifier for further research. For example, Rogers RT/duroid 6002 substrate has a dielectric constant of 2.94 and dielectric loss tangent of 0.0012 that is less than one tenth of that of FR-4 substrate. The dielectric conductivity can then be much lower than what we have in FR-4, allowing accurate microstrip transmission line matching with small deviations of center frequency.

### Bandwidth and matching network

For an ambient RF power harvester, a wider bandwidth is usually desired as the power excitation collected from environments might come from multiple sources communicating in different frequency channels.

In this design, a tapped capacitor transformer with discrete LC components is implemented for impedance matching since tunable capacitors are much easier for matching design on various conditions (incident power, load resistance). However, the quality factor of those capacitors decreases rapidly to a value less than 5 at desired frequency of 2.45 GHz (illustrated in Table 3). As a result, the overall performance of power harvesting circuits can significantly degrade. Meanwhile, microstrip transmission line matching is not ideal for the substrate material with high dielectric loss.

Above all, two possible solutions can be conducted in further research. The one is that, with a better PCB substrate material, microstrip matching is preferred. Considering a broadband situation, radial stub is the potential choice for the design of matching networks, which have been demonstrated in [1]. The other one is to replace discrete components by tunable capacitors with different technologies, such as RF-MEMS capacitors, which are characterized by high-Q and high-tuning-ranges. For instance, [44] has demonstrate an RF-MEMS fractal capacitor [45] with high SRFs. Measured quality factors are higher than 4 throughout the band of 1–15 GHz and reach 18 at 2.5 GHz and as high as 28 at 5 GHz. Theoretically, this type of capacitor is a potential substitute for variable capacitors with low quality factors at high frequencies in our design.

**Discontinuous waveforms**

In the category of this thesis, all that is concerned and studied on continuous waveforms generated from an RF signal generator. However, as is known to us all, a most commonly existing energy source type in 2.4 – 2.5 GHz band is Wi-Fi transmitter. Wi-Fi signals often show the waveform with discrete data transmission, which can be problems for RF energy awareness and activation of cold start circuit in boost converter module. Thus, another promising topic in future works may concentrate on waveform awareness and processing in an RF harvesting system.

**Intrinsic improvement**

The future works mentioned above can improve the performance of the RF energy harvester in this work, but cannot completely solve the problem of low PCE at micro-power region. To essentially increase the PCE and improve the power sensitivity of RF energy harvester, some further solutions are discussed here.

In order to increase the PCE at low power region, the topic in further studies is to focus on the structure of diodes. As we can see in the expression of parasitic efficiency (8), zeros-bias junction resistance $R_{j0}$ and parasitic series resistance $R_s$ play a key role in the overall power conversion efficiency. As is mentioned in section 4.1.4, there is a tradeoff between RF-to-DC efficiency that requires a higher $R_{j0}$ and parasitic efficiency that rather prefers a lower $R_{j0}$. Therefore, a diode structure with tunable junction resistance is desired, which can be achieved by special diodes, such as the spindiode [12],[13]. As for parasitic series resistance $R_s$ and package losses, structure of rectifying diodes should be concerned and special care should be given during the fabrication process. For example, the backward tunneling diode mentioned in [13], [14] can be a good substitute because of the breakthrough of zero-bias current responsivity of Schottky diodes [14].

On the other hand, to improve the power sensitivity of the RF harvesting system. The first option is to combine the power of multiple power harvesters by building a rectenna array instead of use a single rectifier. The work [1] has already proposed a high performance power harvester that integrates nine identical rectifiers with a minimum sensitivity of -40 dBm. Another solution is to concentrate on the design of the boost converter module. The activation of boost converter requires a high power and voltage because of the threshold of a JFET or MOSFET [10], [17]. The future topic can be the modification of the structure of boost converter or the studies of a JFET or MOSFET with lower threshold for the boost converter.

## Reference

[1] U. Olgun, C. c Chen, and J. L. Volakis, “Design of an efficient ambient WiFi energy harvesting system,” *Antennas Propagation IET Microwaves*, vol. 6, no. 11, pp. 1200–1206, Aug. 2012.

[2] Z. Popovic, “Cut the Cord: Low-Power Far-Field Wireless Powering,” *IEEE Microwave Magazine*, vol. 14, no. 2, pp. 55–62, Mar. 2013.

[3] W. C. Brown, “The history of power transmission by radio waves”, *IEEE Trans. Microw. Theory Tech.*, vol. 32, pp. 1230–1242, Sept. 1984.

[4] H.c Sun, *Far-Field Wireless Power Transmission and Ambient RF Energy Harvesting: Concepts, Designs, Applications*. Scholar’s Press, August 7, 2015

[5] M. Piñuela, P. D. Mitcheson, and S. Lucyszyn, “Ambient RF Energy Harvesting in Urban and Semi-Urban Environments,” *IEEE Transactions on Microwave Theory and Techniques*, vol. 61, no. 7, pp. 2715–2726, Jul. 2013.

[6] Naoki Shinohara, *Wireless Power Transfer via Radiowaves*. Wiley-ISTE; 1st edition, Jan. 28, 2014

[7] M. M. Ollivier, “RFID-a practical solution for problems you didn’t even know you had!,” in *IEE Colloquium on Wireless Technology (Digest No. 1996/199)*, 1996, p. 3/1-3/6.

[8] R. J. M. Vullers, R. v Schaijk, H. J. Visser, J. Penders, and C. V. Hoof, “Energy Harvesting for Autonomous Wireless Sensor Networks,” *IEEE Solid-State Circuits Magazine*, vol. 2, no. 2, pp. 29–38, Spring 2010.

[9] K. Gudan, S. Chemishkian, J. J. Hull, S. J. Thomas, J. Ensworth, and M. S. Reynolds, “A 2.4GHz ambient RF energy harvesting system with -20dBm minimum input power and NiMH battery storage,” in *2014 IEEE RFID Technology and Applications Conference (RFID-TA)*, 2014, pp. 7–12.

[10] K. Gudan, S. Shao, J. J. Hull, J. Ensworth, and M. S. Reynolds, “Ultra-low power 2.4GHz RF energy harvesting and storage system with -25dBm sensitivity,” in *2015 IEEE International Conference on RFID (RFID)*, 2015, pp. 40–46.

[11] K. Gudan, S. Shao, J. J. Hull, A. Hoang, J. Ensworth, and M. S. Reynolds, “Ultra-low power autonomous 2.4GHz RF energy harvesting and storage system,” in *2015 IEEE International Conference on RFID Technology and Applications (RFID-TA)*, 2015, pp. 176–181.

[12] S. Hemour *et al.*, “Towards Low-Power High-Efficiency RF and Microwave Energy Harvesting,” *IEEE Transactions on Microwave Theory and Techniques*, vol. 62, no. 4, pp. 965–976, Apr. 2014.

[13] S. Hemour and K. Wu, “Radio-Frequency Rectifier for Electromagnetic Energy Harvesting: Development Path and Future Outlook,” *Proceedings of the IEEE*, vol. 102, no. 11, pp. 1667–1691, Nov. 2014.

[14] C. H. P. Lorenz *et al.*, “Breaking the Efficiency Barrier for Ambient Microwave Power Harvesting With Heterojunction Backward Tunnel Diodes,” *IEEE Transactions on Microwave Theory and Techniques*, vol. 63, no. 12, pp. 4544–4555, Dec. 2015.

[15] S. E. Adami, V. Marian, N. Degrenne, C. Vollaire, B. Allard, and F. Costa, “Self-powered ultra-low power DC-DC converter for RF energy harvesting,” in *2012 IEEE Faible Tension Faible Consommation*, 2012, pp. 1–4.

[16] J.M. Damaschke, “Design of a low-input-voltage converter for thermoelectric generator,” *IEEE Transactions on Industry Applications*, vol. 33, 1997, pp. 1203-1207.

[17] M. Pollak, L. Mateu, and P. Spies, “Step-up DC-DC-Converter with coupled inductors for low input voltages,” *Fraunhofer IIS, 2008*.vol. 86, May. 2011, pp. 625-632.

[18] F. Giuppi, K. Niotaki, A. Collado, and A. Georgiadis, “Challenges in energy harvesting techniques for autonomous self-powered wireless sensors,” in *2013 European Microwave Conference*, 2013, pp. 854–857.

[19] V. Talla, S. Pellerano, H. Xu, A. Ravi, and Y. Palaskas, “Wi-Fi RF energy harvesting for battery-free wearable radio platforms,” in *2015 IEEE International Conference on RFID (RFID)*, 2015, pp. 47–54.

[20] X. Lu, P. Wang, D. Niyato, D. I. Kim, and Z. Han, “Wireless Networks With RF Energy Harvesting: A Contemporary Survey,” *IEEE Communications Surveys Tutorials*, vol. 17, no. 2, pp. 757–789, Secondquarter 2015.

[21] C. M. Ghiglino, “Ultra-Wideband (UWB) Rectenna Design for Electromagnetic Energy Harvesting,” M.S. thesis, Dept. Teoria del Senyal i Comun., Escola Técnica Superior d'Enginyeria de Telecomun, de Barcelona, Catalunya, Spain, 2010.

[22] R. Moghe, Y. Yang, F. Lambert, and D. Divan, “A scoping study of electric and magnetic field energy harvesting for wireless sensor networks in power system applications,” in *2009 IEEE Energy Conversion Congress and Exposition*, 2009, pp. 3550–3557.

[23] H. J. Visser, A. C. F. Reniers, and J. A. C. Theeuwes, “Ambient RF Energy Scavenging: GSM and WLAN Power Density Measurements,” in *2008 38th European Microwave Conference*, 2008, pp. 721–724.

[24] U. Karthaus and M. Fischer, “Fully integrated passive UHF RFID transponder IC with 16.7- mu;W minimum RF input power,” *IEEE Journal of Solid-State Circuits*, vol. 38, no. 10, pp. 1602–1608, Oct. 2003.

[25] A. Shameli, A. Safarian, A. Rofougaran, M. Rofougaran, and F. D. Flaviis, “Power Harvester Design for Passive UHF RFID Tag Using a Voltage Boosting Technique,” *IEEE Transactions on Microwave Theory and Techniques*, vol. 55, no. 6, pp. 1089–1097, Jun. 2007.

[26] N. Soltani and F. Yuan, “A High-Gain Power-Matching Technique for Efficient Radio-Frequency Power Harvest of Passive Wireless Microsystems,” *IEEE Transactions on Circuits and Systems I: Regular Papers*, vol. 57, no. 10, pp. 2685–2695, Oct. 2010.
[27] J. Y. Park, S. M. Han, and T. Itoh, “A rectenna design with harmonic rejecting circular-sector antenna,” *IEEE Antennas Wireless Propag. Lett.* , vol. 3, pp. 52–54, 2004.
[28] “Dengyo rectennas,” Nihon Dengyo Kosaku Company Ltd., Tokyo, Japan, Jul. 2012. Available: http://www.den-gyo.com/solution/solution01.html
[29] “2.4-GHz Inverted F Antenna”, Texas Instruments Inc., Apr. 2007, Revised Feb. 2017. Available: http://www.ti.com/lit/an/swru120c/swru120c.pdf
[30] S. Kim et al., “Ambient RF Energy-Harvesting Technologies for Self-Sustainable Standalone Wireless Sensor Platforms,” *Proceedings of the IEEE*, vol. 102, no. 11, pp. 1649–1666, Nov. 2014.
[31] G. Andia Vera, A. Georgiadis, A. Collado, and S. Via, “Design of a 2.45 GHz rectenna for electromagnetic (EM) energy scavenging,” in *2010 IEEE Radio and Wireless Symp. (RWS)*, 2010, pp. 61 – 64.
[32] K. Lui, A. Vilches, and C. Toumazou, “Ultra-efficient microwave harvesting system for battery-less micropower microcontroller platform,” *IET Microw., Antennas & Propag.*, vol. 5, pp. 811 – 817, 2011.
[33] A. M. Niknejad and A.M. Niknejad, *Electromagnetics for High-Speed Analog and Digital Communication Circuits.* Cambridge, U.K.: Cambridge Univ. Press, 2007.
[34] C. H. P. Lorenz, S. Hemour, and K. Wu, “Physical Mechanism and Theoretical Foundation of Ambient RF Power Harvesting Using Zero-Bias Diodes,” *IEEE Transactions on Microwave Theory and Techniques*, vol. 64, no. 7, pp. 2146–2158, Jul. 2016.
[35] “SMS7630 Series, Surface Mount Mixer and Detector Schottky Diodes”, Skyworks Solutions, Inc., Jul. 2016. Available: http://www.skyworksinc.com/Product/511/SMS7630_Series
[36] S. Mandal and R. Sarpeshkar, “Low-Power CMOS Rectifier Design for RFID Applications,” *IEEE Transactions on Circuits and Systems I: Regular Papers*, vol. 54, no. 6, pp. 1177–1188, Jun. 2007.
[37] A. Georgiadis, G. V. Andia, and A. Collado, “Rectenna design and optimization using reciprocity theory and harmonic balance analysis for electromagnetic (EM) energy harvesting,” IEEE Antennas and Wireless Propagation Letters, vol. 9, pp. 444–446, 2010.
[38] John S. Seybold, *Introduction to RF propagation*. John Wiley & Sons, Inc. 2005. Eq.(2.6), p.22.
[39] C. H. P. Lorenz, S. Hemour, and K. Wu, “Modeling and influence of matching network insertion losses on ambient microwave power harvester,” in *2015 IEEE MTT-S International*

*Conference on Numerical Electromagnetic and Multiphysics Modeling and Optimization (NEMO)*, 2015, pp. 1–3.
[40] “bq25570 Nano Power Boost Charger and Buck Converter for Energy Harvester Powered Applications”, Texas Instruments Inc. Mar. 2013, revised Mar, 2015. Available: http: //www.ti.com/lit/ds/symlink/bq25570.pdf
[41] K. W. Lui, A. Vilches, and C. Toumazou, “Ultra-efficient microwave harvesting system for battery-less micropower microcontroller platform,” *Antennas Propagation IET Microwaves*, vol. 5, no. 7, pp. 811–817, May 2011.
[42] U. Karthaus and M. Fischer, “Fully integrated passive UHF RFID transponder IC with 16.7- µW minimum RF input power,” *IEEE Journal of Solid-State Circuits*, vol. 38, no. 10, pp. 1602–1608, Oct. 2003.
[43] N. Soltani and F. Yuan, “A High-Gain Power-Matching Technique for Efficient Radio-Frequency Power Harvest of Passive Wireless Microsystems,” *IEEE Transactions on Circuits and Systems I: Regular Papers*, vol. 57, no. 10, pp. 2685–2695, Oct. 2010.
[44] A. M. Elshurafa, A. G. Radwan, A. Emira, and K. N. Salama, “RF MEMS Fractal Capacitors With High Self-Resonant Frequencies,” *Journal of Microelectromechanical Systems*, vol. 21, no. 1, pp. 10–12, Feb. 2012.
[45] H. Samavati, A. Hajimiri, A. Shahani, G. Nasserbakht, and T. Lee, “Fractal Capacitors,” IEEE International Solid State Circuits Conference, 256-257, 1998.